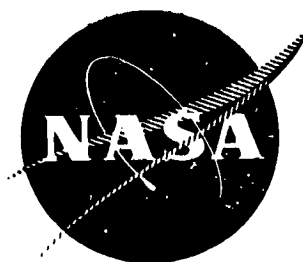


NASA CR - 135019



DOUBLE ION PRODUCTION IN MERCURY THRUSTERS

(NASA-CR-135019) DOUBLE ION PRODUCTION IN  
MERCURY THRUSTERS M.S. Thesis (Colorado  
State Univ.) 86 p HC \$5.00 CSCL 210

N76-22299

Unclas  
G3/20 26906

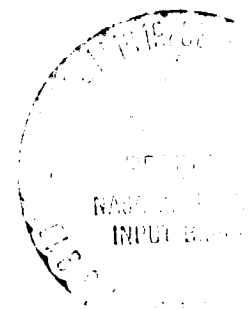
PREPARED FOR  
LEWIS RESEARCH CENTER  
NATIONAL AERONAUTICS AND SPACE ADMINISTRATION  
Grant NGR-06-002-112

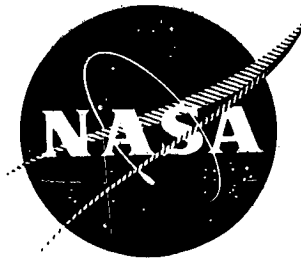
by

Ralph R. Peters

Approved by  
Paul J. Wilbur  
April 1976

Department of Mechanical Engineering  
Colorado State University  
Fort Collins, Colorado





DOUBLE ION PRODUCTION IN MERCURY THRUSTERS

PREPARED FOR  
LEWIS RESEARCH CENTER  
NATIONAL AERONAUTICS AND SPACE ADMINISTRATION  
Grant NGR-06-002-112

by  
Ralph R. Peters

Approved by  
Paul J. Wilbur  
April 1976  
Department of Mechanical Engineering  
Colorado State University  
Fort Collins, Colorado

1. Report No. NASA CR - 135019		2. Government Accession No.		3. Recipient's Catalog No.	
4. Title and Subtitle DOUBLE ION PRODUCTION IN MERCURY THRUSTERS				5. Report Date May, 1976	
				6. Performing Organization Code	
7. Author(s) Ralph R. Peters and Paul J. Wilbur				8. Performing Organization Report No.	
9. Performing Organization Name and Address Department of Mechanical Engineering Colorado State University Fort Collins, Colorado 80523				10. Work Unit No.	
				11. Contract or Grant No. NGR-06-002-112	
12. Sponsoring Agency Name and Address National Aeronautics and Space Administration Washington, D. C. 20546				13. Type of Report and Period Covered	
				14. Sponsoring Agency Code	
15. Supplementary Notes Grant Monitor - William Kerslake, NASA Lewis Research Center, Cleveland, Ohio 44135. This report is a reproduction of the M.S. Thesis of Mr. Ralph R. Peters. It is submitted to the sponsor and to the distribution list in this form both as a presentation of the technical material, and as an indication of the academic program supported by this Grant.					
16. Abstract  Significant densities of doubly charged ions exist in the discharge chambers of electron bombardment ion thrusters. These ions are undesirable because they are a major plasma constituent effecting the sputtering damage which limits thruster lifetime. It would be desirable to reduce their density while maintaining good thruster performance. The development of a model which predicts the doubly charged ion density is discussed. The accuracy of the model is shown to be good for two different thruster sizes and a total of 11 different cases. The model indicates that in most cases more than 80% of the doubly charged ions are produced from singly charged ions. This result can be used to develop a much simpler model which, along with correlations of the average plasma properties, can be used to determine the doubly charged ion density in ion thrusters with acceptable accuracy. Two different techniques which can be used to reduce the doubly charged ion density, while maintaining good thruster operation, are identified as a result of an examination of the simple model. First, the electron density can be reduced and the thruster size then increased to maintain the same propellant utilization. Second, at a fixed thruster size, the plasma density, temperature and energy can be reduced and then to maintain a constant propellant utilization the open area of the grids to neutral propellant loss can be reduced through the use of a small hole accelerator grid. The reduction in the values of the plasma properties causes a decrease in the doubly charged ion density.					
17. Key Words (Suggested by Author(s)) Electrostatic Thruster Mercury Discharge Chamber Model				18. Distribution Statement Unclassified - Unlimited	
19. Security Classif. (of this report) Unclassified		20. Security Classif. (of this page) Unclassified		21. No. of Pages 35	
				22. Price*	

\* For sale by the National Technical Information Service, Springfield, Virginia 22161

## TABLE OF CONTENTS

	<u>Page</u>
ABSTRACT . . . . .	i
TABLE OF CONTENTS . . . . .	ii
LIST OF TABLES . . . . .	iii
LIST OF FIGURES . . . . .	iii
INTRODUCTION . . . . .	1
THRUSTER OPERATION . . . . .	2
THEORETICAL MODEL . . . . .	6
Introduction . . . . .	6
Electron Bombardment Reactions . . . . .	10
Migration Losses . . . . .	16
Photon Diffusion Losses . . . . .	19
Determination of Specie Densities . . . . .	21
EXPERIMENTAL PROCEDURES AND RESULTS . . . . .	24
RESULTS AND DISCUSSION . . . . .	32
SIMPLIFIED MODEL . . . . .	39
CONCLUSIONS . . . . .	55
REFERENCES . . . . .	56
APPENDIX A: Listing of the Computer Program HG . . . . .	58
APPENDIX B: Listing of the Computer Program PROP . . . . .	73

## LIST OF TABLES

<u>Table Number</u>	<u>Page</u>
I Thruster Sizes, Configurations and Conditions . . . . .	26
II Experimental Results . . . . .	29
III Predicted Densities and Reaction Rates . . . . .	36
IV Determination of the Double Ion Density Using the Simplified Model . . . . .	51

## LIST OF FIGURES

<u>Figure Number</u>	<u>Page</u>
1 Electron Bombardment Ion Thruster Schematic . . . . .	3
2 Discharge Chamber Reaction Schematic . . . . .	7
3 Mercury Cross Sections . . . . .	12
4 Plasma Property Profiles, 15 cm Thruster - SERT II Grids - 37 V Anode Voltage . . . . .	28
5 Double-to-Single Ion Density Ratio in a 15 cm Diameter Thruster . . . . .	33
6 Double-to-Single Ion Density Ratio in a 30 cm Diameter Thruster . . . . .	34
7 Rate Factors for $Hg^+ \rightarrow Hg^{++}$ . . . . .	41
8 Maxwellian Electron Temperature Correlation . . . . .	43
9 Primary Electron Energy Correlation . . . . .	45
10 Electron Density Correlation . . . . .	47
11 Primary Electron Density Correlation . . . . .	48
12 Uniformity Factor Correlation . . . . .	49

## INTRODUCTION

Electron bombardment ion thrusters are presently being considered for use in deep space probes and for satellite stationkeeping functions. These devices which have the advantage of very high specific impulses also have the attendant disadvantage of low thrust densities. This low thrust characteristic necessitates thruster operation for long periods of time in order to accomplish typical missions (of the order of 10,000 hours). Thruster lifetimes can be limited by the erosion of ion chamber component parts with most of this erosion (or sputtering damage) being caused by doubly charged ions. Long thruster lifetimes therefore require control of doubly charged ion densities.

Many experiments could be performed to determine how the thruster should be operated so that thruster performance would be good and the doubly charged ion density would be reduced to an acceptable level. However, these experiments would have the disadvantage of being time consuming and costly and the results might be applicable to one size and type of thruster only. Instead a theoretical model could be developed which would accurately predict the doubly charged ion density over a wide range of conditions and thruster sizes. This model could be applied at low cost to determine the factors affecting the doubly charged ion density and how they should be adjusted to reduce the double ion density. It should also indicate what effects these changes would have on thruster performance. Such a model has been developed for electron bombardment ion thrusters and has been verified experimentally for thrusters which use mercury propellant. A discussion of the model's development and verification is presented in this paper along with some results and conclusions based upon the model.

## THRUSTER OPERATION

Many of the assumptions and approximations used in the development of the model are based upon a knowledge of thruster operation. This section will briefly discuss thruster operation so that the development of the model in the next section will be more easily understood. An ion thruster has two basic tasks to perform:

- 1) Ionization of the neutral propellant atoms.
- 2) Acceleration of the ions to high velocities producing thrust.

These two topics will form the basis for the discussion of thruster operation.

Figure 1 shows a schematic for a typical electron bombardment ion thruster. The specific type shown has a strongly divergent magnetic field which is presently the most common type. However, the operation of all types of electron bombardment ion thrusters is very similar<sup>(1)</sup>. Electrons are emitted from the cathode and are drawn toward the anode which is biased 30-40V positive with respect to the cathode. These electrons (called primary electrons) are injected into the primary electron region with an energy slightly less than that associated with the 30-40V anode voltage. Electrons in this region are kept from going immediately to the anode by a magnetic field set up between the cathode pole piece and the anode pole piece but collisions eventually facilitate electron diffusion across these magnetic field lines so that they can be collected by the anode. As a result of the magnetic field containment the electron density is much higher ( $\sim 10^{11} \text{ cm}^{-3}$ ) within this region than it is outside of it. The primary electron region's boundary is defined by the surface of revolution of the critical (magnetic) field line and the screen grid. Because the strength of the magnetic field

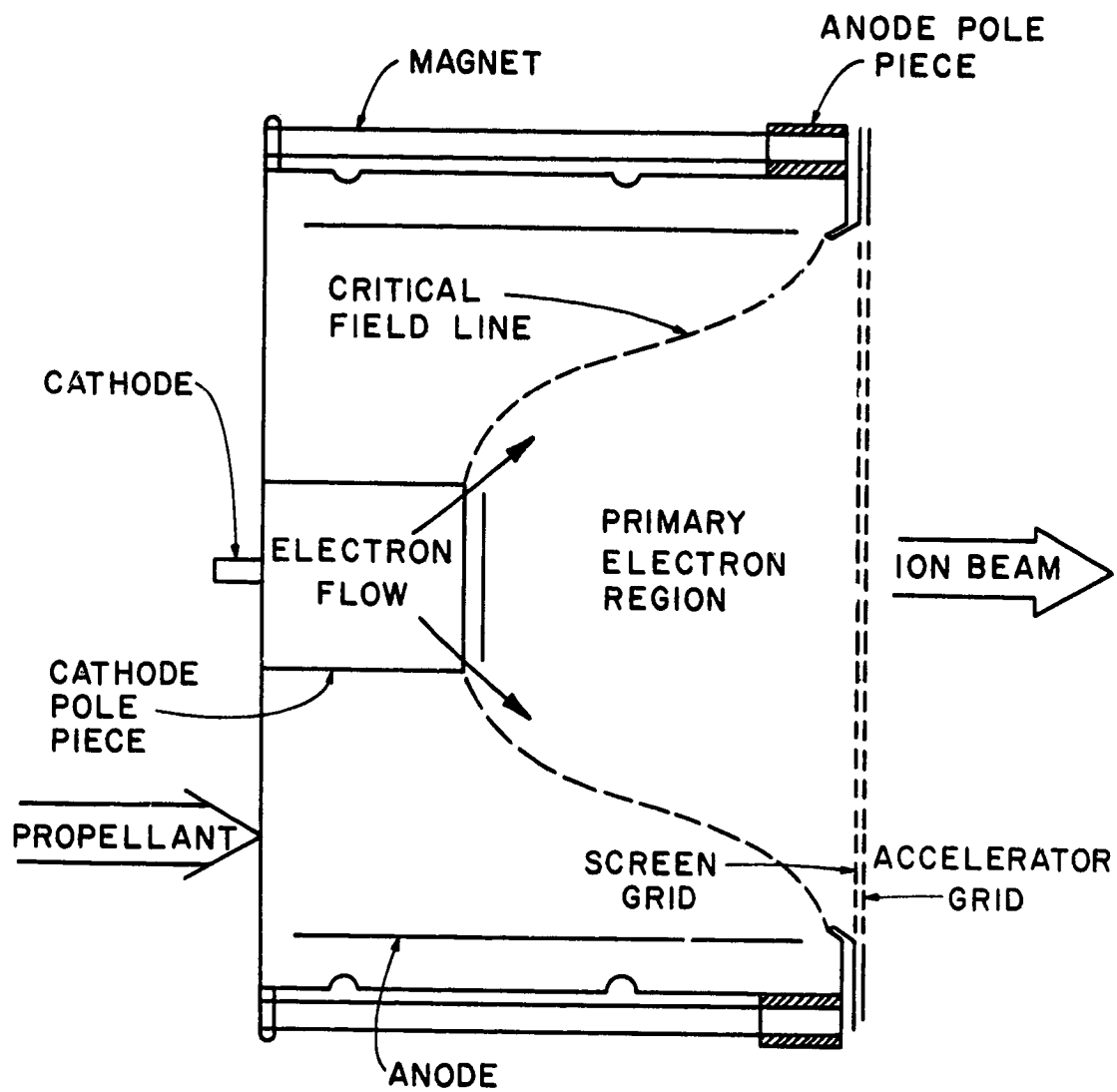


Figure 1 Electron Bombardment Ion Thruster Schematic



is fairly low within it, a fairly uniform electron density exists throughout the entire region.

Neutral propellant (e.g. mercury) is injected into the upstream end of the discharge chamber at low pressure ( $10^{-4}$  torr). Most of the interactions between electrons and neutral propellant atoms take place in the primary electron region because higher electron densities and energies exist there. Electrons bombard the neutral atoms occasionally knocking an outer shell electron loose from the atom forming a singly charged ion. The production of a mercury single ion requires more than 10 eV of energy from the incident electron. This electron and the ejected electron then share the remainder of the energy which the incident electron carried originally. This reaction results in the replacement of one high energy electron with two lower energy electrons which rapidly randomize with similarly generated electrons to form a Maxwellian electron group. Ions are extracted from the plasma through holes in the screen and accelerator grids as a result of the large potential difference applied across these two grids. The rate of ion loss through the grids times the ionic charge is called the beam current.

Electron bombardment of atoms and ions also produces doubly charged ions. Many of these ions are extracted from the discharge chamber by the grids, however, some of them go to the walls. As ions near the walls (the cathode pole piece, screen grid, etc.) they are accelerated to high velocities by an electric field that exists at the plasma boundary. When these high velocity ions strike the walls they can knock atoms loose (sputter atoms) from the walls of the discharge chamber. The energy that doubly charged ions possess upon striking the

walls is twice that of singly charged ions, therefore the sputtering damage caused by a double ion is much greater than that caused by a single ion. Double ions are thought to cause most of the sputtering damage even though their density is typically an order of magnitude less than that of the single ions.

## THEORETICAL MODEL

### Introduction

In order to develop a simple model for determining the double ion density in the discharge chamber only those ionic and atomic species which were considered significant in determining the double ion density were included. The significant species were selected as those which have substantial electron impact cross sections of formation over the electron energy range of interest so that large numbers of these excited atoms or ions will be produced. These states also have sufficiently long effective lifetimes so that they can participate in production processes before they decay. Only those reactions which lead directly or indirectly to the production of double ions were included.

Figure 2 is a discharge chamber reaction schematic showing these dominant species and the reactions in which each specie can participate. The model has been developed for thrusters using mercury propellant but the general procedure is valid for thrusters using other propellants.

The symbols used in Figure 2 represent the following species:

$\text{Hg}^0$  - neutral ground state mercury

$\text{Hg}^m$  - metastable neutral mercury ( $6^3P_0$  and  $6^3P_2$  states)

$\text{Hg}^r$  - resonance state neutral mercury ( $6^3P_1$  and  $6^1P_1$  states)

$\text{Hg}^+$  - singly ionized ground state mercury

$\text{Hg}^{m+}$  - singly ionized metastable mercury ( $6^2D_{3/2}$  and  $6^2D_{5/2}$  states)

$\text{Hg}^{++}$  - doubly ionized ground state mercury

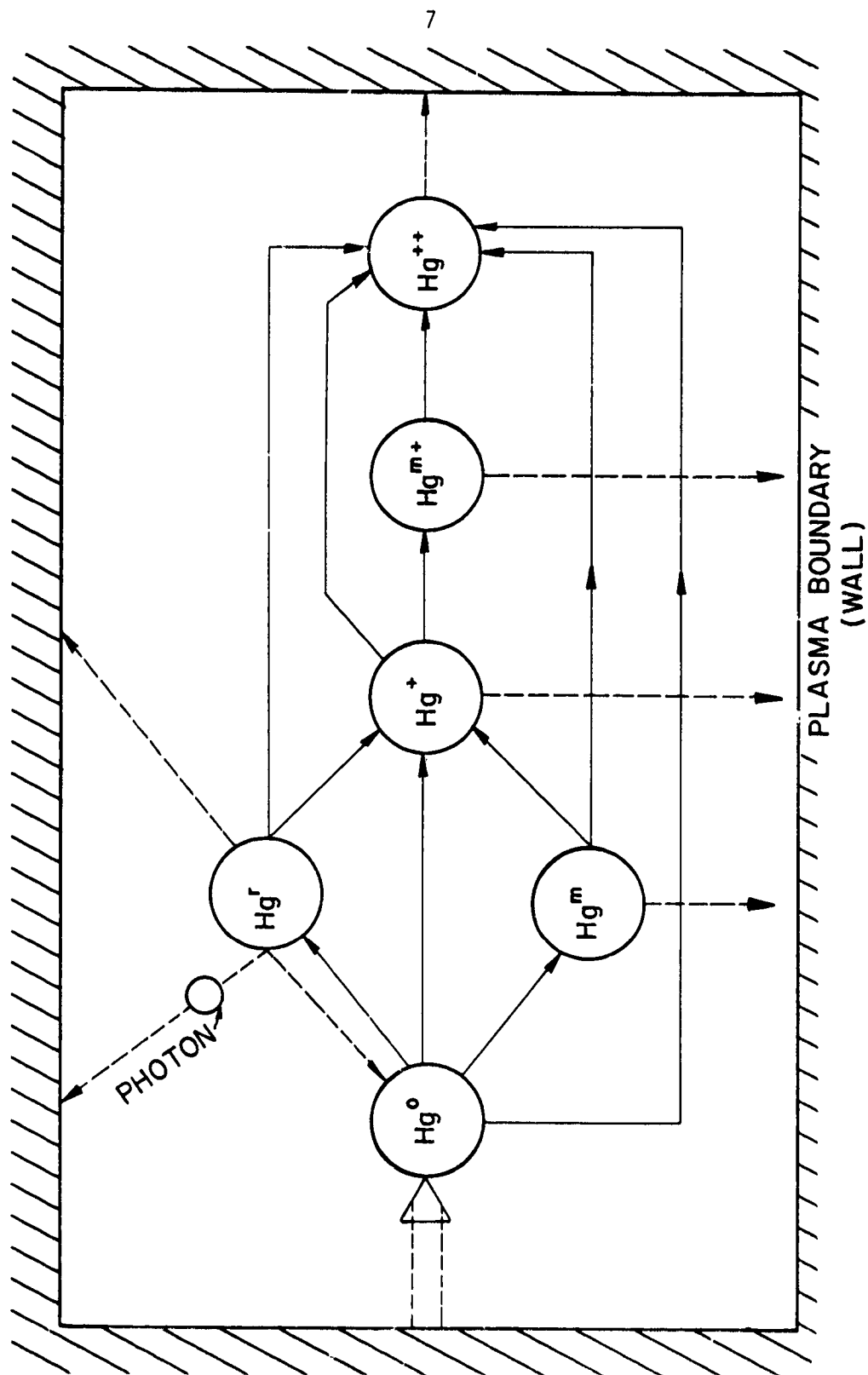


Figure 2 Discharge Chamber Reaction Schematic

The arrows in Figure 2 indicate the various interaction routes considered in this analysis. Three different types of reactions are indicated in this figure. The first type of reaction occurs when an electron interacts with an atom or ion producing a more highly excited specie. This reaction is indicated in Figure 2 by an arrow going from one specie to another more highly excited specie (e.g. the production of double ions from single ions). The production of a highly excited specie also represents a loss mechanism for the less excited specie. The reverse reaction in which, for example, an ion captures an electron is improbable because the reaction requires three bodies to simultaneously collide.

The second type of process is that of an atom or ion going to a plasma boundary. Such a boundary could be either the discharge chamber wall on which the atom or ion would be de-excited or it could be a grid aperture in which case the atom or ion would be extracted from the discharge region. In either case this represents a loss rate for any of the excited states. These losses to the boundary are indicated in Figure 2 by the dotted lines to the wall of the chamber. The large arrow back to the neutral ground state represents the resupply of neutral ground state atoms either from the walls or from the propellant supply system.

A third type of reaction shown in Figure 2 is relevant only to the two resonance states. The resonance states differ from metastable states in that they have a very short lifetime before they de-excite spontaneously by emitting a photon of light. However, the energy of this photon is such that it is readily absorbed by a nearby neutral ground state atom producing another resonance state atom. Since the

transport time of the photon is small compared to the excited state lifetime the excited state can be considered to exist continuously. Eventually the photon can diffuse to a boundary where it will be lost; this is equivalent to the loss of a resonance state atom. This loss mechanism is represented in Figure 2 by a dotted line conveying a photon to the wall and a branching line going from the resonance atom to the neutral ground state atom.

Figure 2 also shows the dominant routes for the production and loss of all of the excited atoms and ions considered. For example, ground state single ions can be produced as a result of electron bombardment of neutral ground-state, resonance state, and metastable state atoms and these single ions can be lost as a result of single ion migration to the plasma boundary and the production of metastable single ions and double ions by electron bombardment.

When equilibrium conditions exist in the discharge chamber the rate of production of each specie must equal its loss rate. If, for example, the production rate of single ions increases, the single ion density must also increase to keep the loss rate (which is directly proportional to the single ion density) equal to the higher production rate. This example illustrates the fact that the equilibrium density of any specie is determined by the associated production and loss rates. If equations determining the production and loss rates could be derived, these equations could then be solved for the equilibrium density of any specie under consideration. The remainder of this section is concerned with deriving equations for the production and loss mechanisms indicated in Figure 2 and then solving these equations for the equilibrium densities of the various states.

### Electron Bombardment Reactions

The first reaction to be considered is the one which produces excited atoms or ions by electron bombardment from less excited atoms or ions. The total rate of production of any specie  $\gamma$  from specie  $\alpha$  (and hence the loss rate of  $\alpha$  due to this reaction) is given by:

$$R_{\alpha}^{\gamma} = \int_{\text{Plasma Volume}} \int_{E=0}^{E=\infty} n_{\alpha} \sigma_{\alpha}^{\gamma}(E) v_e(E) dn_e dV \quad (1)$$

where  $n_{\alpha}$  is the density of specie  $\alpha$  at some point  $\vec{r}$  in the plasma,  $\sigma_{\alpha}^{\gamma}(E)$  is the cross section for the production of  $\gamma$  from  $\alpha$  at the electron energy  $E$ <sup>(2-6)</sup>,  $v_e$  is the electron velocity at energy  $E$ ,  $dn_e$  is the density of electrons with energies between  $E$  and  $E + dE$  at  $\vec{r}$ , and  $dV$  is the infinitesimal volume element. The distribution of electrons over the energy spectrum of an ion thruster was assumed to be composed of a Maxwellian electron group which is described by a temperature ( $T_{mx}$  -- eV) and a density ( $n_{mx}$  --  $\text{cm}^{-3}$ ) and a monoenergetic group (primary electrons) which is described by an energy ( $\epsilon_{pr}$  -- eV) and a density ( $n_{pr}$  --  $\text{cm}^{-3}$ ). This type of electron distribution is generally accepted as appropriate for electron bombardment thruster plasmas.<sup>(1,7)</sup>

Substituting this electron distribution into Equation (1) and combining terms to form new functions results in the following equation.

$$R_{\alpha}^{\gamma} = \int_{\text{Volume}} n_{\alpha} [n_{pr} P_{\alpha}^{\gamma}(\epsilon_{pr}) + n_{mx} Q_{\alpha}^{\gamma}(T_{mx})] dV \quad (2)$$

where

$$P_{\alpha}^{\gamma}(\epsilon_{pr}) = v_e(\epsilon_{pr}) \sigma_{\alpha}^{\gamma}(\epsilon_{pr}) \quad (3)$$

and

$$Q_{\alpha}^Y(T_{mx}) = \int_{E=0}^{E=\infty} \sigma_{\alpha}^Y(E) v_e(E) \frac{dn_{mx}(E)}{n_{mx}} . \quad (4)$$

" $[dn_{mx}(E)/n_{mx}]$ " is the Maxwellian distribution function and the other terms are as defined previously.

Where possible the cross sections ( $\sigma_{\alpha}^Y$ ) required for Equations (3) and (4) were selected from experimental data.<sup>(2,3,4)</sup> If experimental data were not available, theoretical cross sections were either obtained from the literature<sup>(5)</sup> or calculated using the Gryzinski approximation.<sup>(6)</sup> The Gryzinski approximation was modified for the cases of the metastable single ion production cross sections to reflect the significant value of the cross sections near the threshold. The cross sections used are presented in Figure 3 along with references indicating their origin.

Using integral equations like Equation (2) in the model would be inconvenient because it would then be very difficult to solve for the density of specie  $\alpha$  ( $n_{\alpha}$ ) since  $n_{\alpha}$  appears within the integral. For this reason it would be desirable to convert Equation (2) into a simple algebraic equation. Fortunately the plasma is fairly uniform in the primary electron region which is where most of the reactions take place. This suggests using average properties in Equation (2) to obtain the following result.

$$R_{\alpha}^Y = n_{\alpha}^* [n_{pr}^* P_{\alpha}^Y(\epsilon_{pr}^*) + n_{mx}^* Q_{\alpha}^Y(T_{mx}^*)] \Psi \quad (5)$$

The asterisks indicate volume averaged quantities and  $\Psi$  is the volume of the primary electron region.



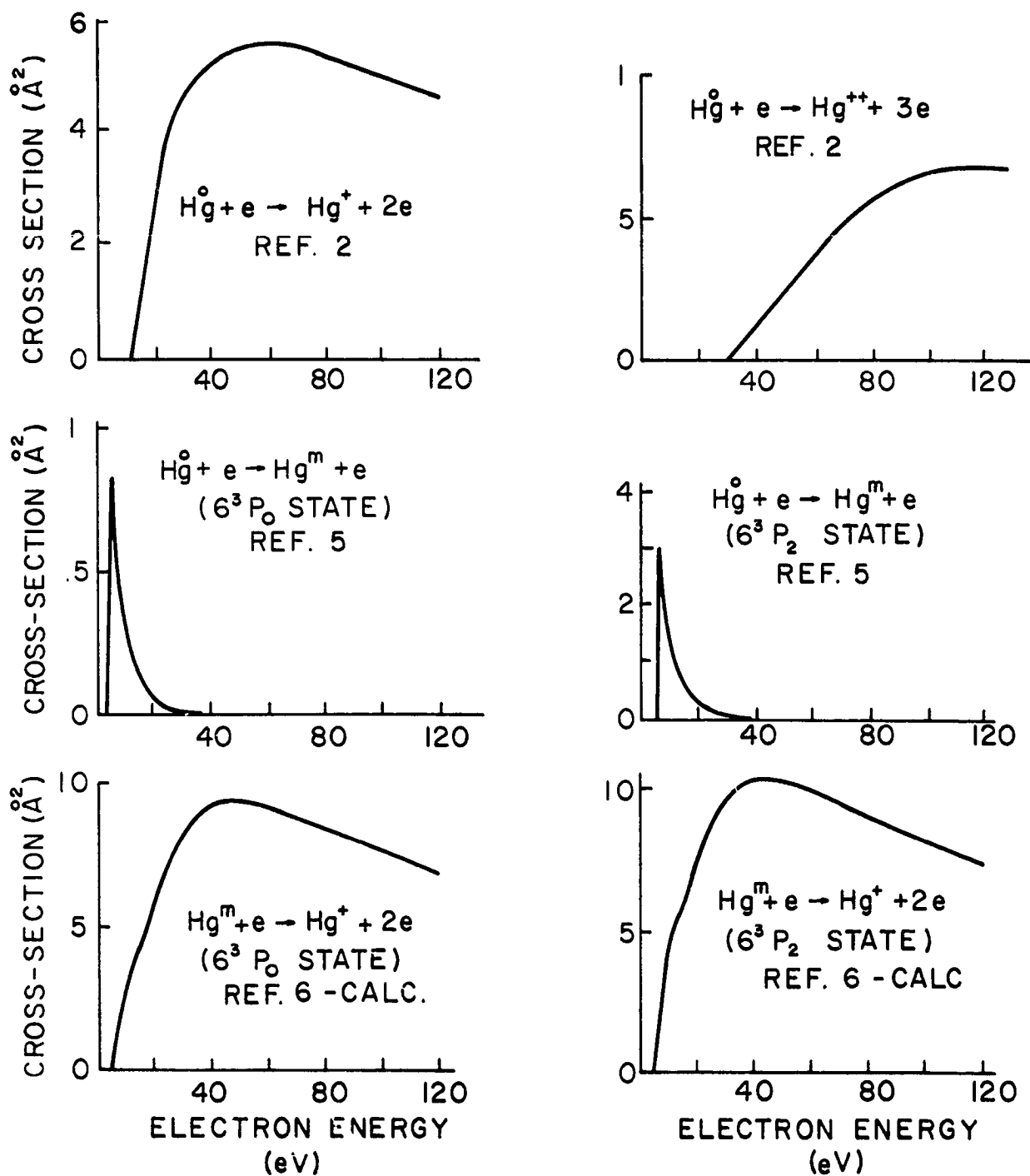


Figure 3 Mercury Cross Sections

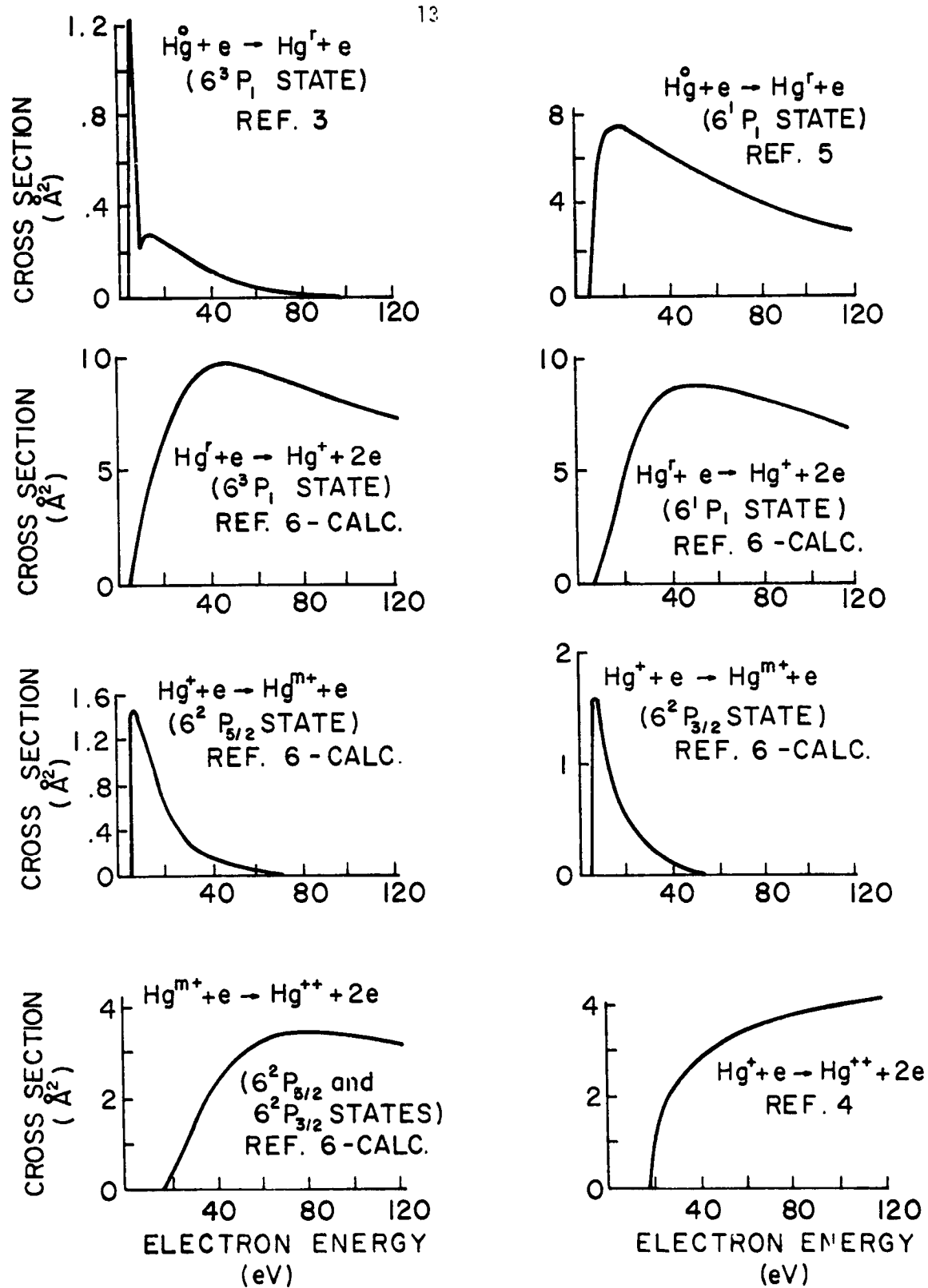


Figure 3 Mercury Cross Sections (continued)

In order to use Equation (5) to evaluate all of the production rates the volume averaged plasma properties ( $n_{pr}^*$ ,  $n_{mx}^*$ ,  $\epsilon_{pr}^*$ ,  $T_{mx}^*$ ) must be determined. Comparing Equations (2) and (5) the following definitions of the volume averaged properties must apply.

$$n_{\alpha}^* n_{pr}^* P_{\alpha}^{\gamma}(\epsilon_{pr}^*) \Psi = \int_{\text{Volume}} n_{\alpha} n_{pr} P_{\alpha}^{\gamma}(\epsilon_{pr}) d\Psi \quad (6)$$

$$n_{\alpha}^* n_{mx}^* Q_{\alpha}^{\gamma}(T_{mx}^*) \Psi = \int_{\text{Volume}} n_{\alpha} n_{mx} Q_{\alpha}^{\gamma}(T_{mx}) d\Psi \quad (7)$$

These two equations show that the volume averaged plasma properties will be weighted in some manner. In order to evaluate the integrals, species  $\alpha$  and  $\gamma$  must be chosen. The only specie density ( $n_{\alpha}$ ) that can be determined readily is the single ion density because plasma neutrality requires it to be approximately equal to the electron density. Specie  $\gamma$  must also be chosen in order to determine what  $P_{\alpha}^{\gamma}$  and  $Q_{\alpha}^{\gamma}$  to use. Figure 2 shows only two choices are possible--the singly ionized metastable states and the doubly ionized ground state. Since the whole purpose of the model is to determine the double ion density, specie  $\gamma$  was chosen as the doubly ionized ground state. Using these choices for species  $\alpha$  and  $\gamma$ , Equations (6) and (7) were rewritten in the following form where the electron density ( $n_e$ ) has been used to approximate the single ion density.

$$n_e^* n_{pr}^* P_+^{++}(\epsilon_{pr}^*) \Psi = \int_{\text{Volume}} n_e n_{pr} P_+^{++}(\epsilon_{pr}) d\Psi \quad (8)$$

$$n_e^* n_{mx}^* Q_+^{++}(T_{mx}^*) \Psi = \int_{\text{Volume}} n_e n_{mx} Q_+^{++}(T_{mx}) d\Psi \quad (9)$$

The volume averaged values of the primary electron energy ( $\epsilon_{pr}^*$ ) and the Maxwellian electron temperature ( $T_{mx}^*$ ) were defined as shown in Equations (10) and (11). These definitions were chosen because they give reasonable values for the properties involved (i.e. these volume averaged values can't be greater than the peak values, which was possible with some of the other definitions).

$$P_+^{++}(\epsilon_{pr}^*) = \frac{\int_{\text{Volume}} n_e n_{pr} P_+^{++}(\epsilon_{pr}) dV}{\int_{\text{Volume}} n_e n_{pr} dV} \quad (10)$$

$$Q_+^{++}(T_{mx}^*) = \frac{\int_{\text{Volume}} n_e n_{mx} Q_+^{++}(T_{mx}) dV}{\int_{\text{Volume}} n_e n_{mx} dV} \quad (11)$$

Equations (8) - (11) along with Equation (12), which says the volume averaged electron density is the sum of the volume averaged primary and Maxwellian electron densities, can be combined to obtain the following definitions of the remaining volume averaged plasma properties.

$$n_e^* = n_{pr}^* + n_{mx}^* \quad (12)$$

$$n_e^* = \left[ \int_{\text{Volume}} n_e^2 dV \right]^{1/2} / V^{1/2} \quad (13)$$

$$n_{pr}^* = \frac{\int_{\text{Volume}} n_e n_{pr} dV}{\left[ \int_{\text{Volume}} n_e^2 dV \right]^{1/2} V^{1/2}} \quad (14)$$

$$n_{mx}^* = \frac{\int_{\text{Volume}} n_e n_{mx} dV}{\left[ \int_{\text{Volume}} n_e^2 dV \right]^{1/2} V^{1/2}} \quad (15)$$

This concludes the mathematical development for electron bombardment reactions.

The volume averaged plasma properties must be evaluated in order to use Equation (5) to calculate the production rates. The plasma properties ( $n_{pr}$ ,  $n_{mx}$ ,  $\epsilon_{pr}$ ,  $T_{mx}$ ) are measured at many points inside the discharge chamber by a Langmuir probe. This data is then used to evaluate the integrals in Equations (10), (11) and (13)-(15) numerically yielding the needed volume averaged plasma properties.

#### Migration Losses

The second type of process to be considered is that of an excited atom or ion going to the plasma boundary. The equation for the plasma boundary loss rate of a specie  $\alpha$  is given by:

$$R_{l\alpha} = \int_{\text{plasma boundary}} n_{\alpha} v_{\alpha} dA \quad (16)$$

where  $n_{\alpha}$  is the density of specie  $\alpha$  at the boundary,  $v_{\alpha}$  is its average velocity toward the plasma boundary, and  $dA$  is the infinitesimal area. For neutral particles assumed to have a temperature equal to the discharge chamber wall temperature and having a mass " $m_0$ " the average velocity toward the boundary ( $v_0$ ) is equal to one-fourth the average thermal speed

$$v_0 = \frac{1}{4} \sqrt{\frac{8k T_{\text{wall}}}{\pi m_0}} \quad (17)$$

where  $k$  is the Boltzmann constant.

For ions this velocity is determined by the Bohm criterion<sup>(8,9)</sup> and is given by

$$v_q = \sqrt{\frac{T_{mx} q}{m_i} \left(1 + \frac{n_{pr}}{n_{mx}}\right)} \quad (18)$$

where  $q$  is the ion charge (coul) and  $m_i$  is the ion mass (kg), and  $T_{mx}$ ,  $n_{pr}$  and  $n_{mx}$  are as defined previously.

Since the integral equation used to define production rates has been reduced to an algebraic equation in terms of average properties Equation (16) should also be simplified in this manner. Because the migration loss is a surface phenomenon, however, it is necessary to use surface averaged densities and velocities based on surface average properties to obtain

$$R_{\ell\alpha} = n_{\alpha}^s v_{\alpha}^s A \quad (19)$$

where  $A$  is the total surface area of the primary electron region and the superscript "s" designates values based on surface averaged properties. Equation (19) could be made more convenient for use in the model if it were based on volume averaged properties as Equation (5) is. Equation (19) was for this reason rewritten in terms of volume averaged densities as follows

$$R_{\ell\alpha} = n_{\alpha}^* v_{\alpha}^* A / F_{\alpha} \quad (20)$$

where  $v_{\alpha}^*$  is  $v_{\alpha}(T_{mx}^*, n_{pr}^*/n_{mx}^*)$  and  $F_{\alpha}$  is a plasma uniformity factor given by Equation (21) which relates the volume and surface averaged density-velocity product.

$$F_{\alpha} = \frac{n_{\alpha}^* v_{\alpha}^*}{n_{\alpha}^s v_{\alpha}^s} = \frac{n_{\alpha}^* v_{\alpha}^*}{\left[ \int_{\text{plasma boundary}} n_{\alpha}^* v_{\alpha}^* dA \right] / A} \quad (21)$$

This concludes the mathematical development for the migration loss of excited species, but some additional discussion and quantification of the uniformity factor  $F_{\alpha}$  is necessary before it can be used in Equation (20). The evaluation of  $F_{\alpha}$  for neutral excited states is difficult because it is difficult to measure their densities. The migration of excited neutrals to the plasma boundary is however a minor loss mechanism compared to the losses due to the conversion of neutral excited atoms into single ions. Therefore  $F_{\alpha}$  for neutral excited states can be set equal to unity without introducing a significant error into the total loss rate calculation. In the case of ions, however, migration to the boundary is a major loss mechanism and  $F_{\alpha}$  must be evaluated in order to obtain accurate results. For the singly ionized ground state the approximation,  $n_{+} = n_e$ , can again be used in order to evaluate  $F_{+}$  using Equation (21). The uniformity factor for the singly ionized metastable states was set to unity since these states have a very minor effect on the double ion density. The determination of  $F_{++}$  is based on the observation<sup>(10)</sup> that the volume averaged double ion density ( $n_{++}^*$ ) is proportional to the volume averaged electron density squared ( $n_e^*$ )<sup>2</sup>. It has been assumed that this proportionality holds locally and this results in the following definition of  $F_{++}$ .

$$F_{++} = \frac{(n_e^*)^2 v_{++}^*}{\left[ \int_{\text{plasma boundary}} n_e^* v_{++}^* dA \right] / A} \quad (22)$$

### Photon Diffusion Losses

The third type of process to be considered is the loss of resonance state atoms due to photon diffusion to the walls of the discharge chamber. From diffusion theory the rate of photon loss across any plasma boundary and hence the rate of resonance state atom loss by this mechanism is given by the equation

$$R_{\text{er}} = \int_{\text{plasma boundary}} D \Delta n_p \, dA = DA[\Delta n_p] \quad (23)$$

In this equation  $n_p$  is the photon density and  $D$  is the photon diffusion coefficient which is given by

$$D = \frac{1}{3\tau(n_0^* \sigma_c)^2} \quad (24)$$

" $\tau$ " in this equation is the average lifetime of the resonance state atom,  $n_0^*$  is the neutral ground state atom density, and  $\sigma_c$  is the cross section for absorption of the photons by neutral ground state atoms. (11)

The second equality in Equation (23) reflects the fact that average properties are being used in this analysis. The photon density has been assumed constant up to a point one photon mean free path from the boundary. From this point the density is assumed to decay linearly to zero at the boundary. This assumption yields the following conservative estimate for the photon loss rate

$$R_{\text{er}} = DA n_p^* / \ell_f \quad (25)$$

where  $\ell_f$  is the mean free path for photon absorption  $(\frac{1}{n_0^* \sigma_c})$ . This



approximation is valid when the photon mean free path is much less than the characteristic dimension of the plasma, a condition that is readily satisfied for this case where the photon mean free paths are very small ( $\lambda_f < .1$  cm).

Since the neutral density is assumed uniform over the discharge region the photon density profile is similar to the resonance state atom density profile and the following approximation between the photon and resonance state atom density at any location in the plasma applies:

$$n_p = n_r \beta \quad (26)$$

$\beta$  is a proportionality constant that can be thought of as the ratio of the probability that a photon will be "free" in the plasma to the probability that it will be "bound" forming a resonance state atom. This ratio of probabilities can also be expressed as the ratio of the average lifetime of a free photon ( $\frac{1}{c n_0^* \sigma_c}$ ) to the resonance state atom lifetime ( $\tau$ ). Therefore,  $\beta$  is given by:

$$\beta = \frac{1}{c n_0^* \sigma_c \tau} \quad (27)$$

where  $c$  is the speed of light and the other quantities have already been defined. Combining Equations (25), (26) and (27) one obtains the following equation for the loss rate of resonance state atoms due to photon diffusion:

$$R_{\text{loss}} = \frac{n_r^*}{3c} A \left[ \frac{1}{c n_0^* \sigma_c \tau} \right] \quad (28)$$

### Determination of Specie Densities

The equations derived so far in this section can now be combined to determine the equilibrium density of each specie included in the model. Equations of the form of (5) and (20) -- and (28) for the case of resonance state atoms -- along with the values for the volume averaged plasma properties and the plasma uniformity factors can be used to determine the rates of production and loss for each specie in the plasma. The steady state density of these species can then be calculated by equating their total production rates to their total loss rates. For example, the  $6^3P_0$  metastable atom density is determined by equating the production rate of this metastable atomic state from neutral ground state atoms to the sum of the associated loss rates due to 1) migration to the wall, 2) production of single ions, and 3) the production of double ions, that is

$$\begin{aligned} n_o^* [n_{pr}^* P_o^m(\epsilon_{pr}^*) + n_{mx}^* Q_o^m(T_{mx}^*)] \Psi = \frac{n_m^* v_m^* A}{F_m} \\ + n_m^* [n_{pr}^* P_m^+(\epsilon_{pr}^*) + n_{mx}^* Q_m^+(T_{mx}^*)] \Psi + n_m^* [n_{pr}^* P_m^{++}(\epsilon_{pr}^*) + n_{mx}^* Q_m^{++}(T_{mx}^*)] \Psi. \end{aligned} \quad (29)$$

Solving this for the metastable atom density ratio one obtains

$$\begin{aligned} \frac{n_m^*}{n_o^*} = [n_{pr}^* P_o^m(\epsilon_{pr}^*) + n_{mx}^* Q_o^m(T_{mx}^*)] / \left\{ \frac{v_m^*}{\Psi/A F_m} + [n_{pr}^* P_m^+(\epsilon_{pr}^*) \right. \\ \left. + n_{mx}^* Q_m^+(T_{mx}^*)] + [n_{pr}^* P_m^{++}(\epsilon_{pr}^*) + n_{mx}^* Q_m^{++}(T_{mx}^*)] \right\} \end{aligned} \quad (30)$$

where  $n_m^*$  is the volume average metastable state density and  $v_m^*$  is the average velocity of metastable neutral atoms toward the boundary. A similar type of equation can be derived for each of the other excited states but they are all as complex or more complex than Equation (30).

For example, the equation for the doubly ionized ground state density has eight terms in the numerator. Each of these terms has the same form as the bracketted quantities in the numerator of Equation (30).

The quantity  $\Psi/A$  in the denominator of Equation (30) has an interesting physical interpretation. It is contained in a term which represents the loss rate per unit volume of metastable state atoms to the plasma boundary. This term shows the manner in which the size and shape of the primary electron region enters into the model. For a large thruster  $\Psi/A$  will be large and an ion or excited neutral must, on the average, travel great distances to reach the plasma boundary, and so the loss rate per unit volume of these species will be small. For a small thruster  $\Psi/A$  will be small and on the average the ions and excited species are near the boundary and can reach it readily resulting in a large loss rate of these species per unit volume.

At this point only the relative density of each excited specie ( $n_{\alpha}^*/n_0^*$ ) can be calculated. However one additional fact can be added to the model, the requirement that the plasma be neutral (i.e.,  $n_e^* = n_+^* + n_{m+}^* + 2n_{++}^*$ ). This requirement when added to the relative density equations of the ionized states implies unique single, metastable single and double ion densities. These in turn imply a unique neutral atom density and hence a unique density for each specie considered in the analysis. One must however iterate to arrive at these densities because a neutral ground state atom density must be assumed initially to determine photon loss rates from Equation (28). At the conclusion of the analysis then the calculated ground state atom density must agree with the assumed value.

A computer program has been written which calculates the densities of all the species considered in the model. The densities are calculated by using relative density equations similar to Equation (30) and the plasma neutrality condition. The input needed to make these calculations includes the volume averaged plasma properties, the plasma uniformity factors and the volume-to-surface area ratio of the primary electron region. A listing of this computer program entitled "HG" is included as Appendix A.

## EXPERIMENTAL PROCEDURES AND RESULTS

The model developed in the previous section will predict the specie densities if the volume averaged plasma properties, uniformity factors and geometric quantities, which are collectively called the input parameters, are known. In order to verify the accuracy of the model, data must be gathered so that the model's input parameters can be determined. These input parameters can be used by the model to predict the specie densities which can then be compared to the measured densities to determine the model's accuracy. The model's accuracy has been determined by comparing the measured and predicted double ion densities since the double ion density is the model's main concern.

In order to test the accuracy of the model over a wide range of conditions data were used from different thrusters and operating conditions. The 15 cm diameter SERT II thruster was operated with two different grid sets and at three different power levels in each of these configurations. Data were collected at each condition allowing the accuracy of the model to be verified at six different points. Data for the 30 cm diameter thruster were also obtained from Hughes Research Laboratories<sup>(12)</sup> so that the model could be verified over a wider range of thruster sizes, configurations, and operating conditions. Both thrusters have strongly divergent magnetic fields. Their general configuration and manner of operation have been described in the "Thruster Operation" section. More detailed thruster specifications, etc. are available in the literature.<sup>(9, 13, 14)</sup>

The data gathering procedure for the 15 cm thruster will be used to illustrate the general manner in which the needed data were obtained.

Before the gathering of data could begin thruster operation and flow rates were kept stable for approximately thirty minutes. This insured thruster conditions would change little in the twenty minute period during which the data were obtained. Table I lists the conditions and configurations at which the 15 cm thruster was operated at C.S.U. along with those for the 30 cm thruster as obtained from Hughes Research Laboratories. This table indicates the changes in configuration for both thrusters resulted from using different grid types. The SERT II grids, listed in Table I, are flat grids with hole diameters of  $\approx .4$  cm and in operation are separated by a gap of .23 cm. The high perveance dished grids are dished slightly to prevent the grids from shorting during operation due to their thermal expansion. Their hole diameter is smaller (.25 cm) as is their separation gap (.079). More detailed specifications for the two grid types can be found in Reference 9. The EM (Engineering Model) grids are similar to the high perveance dished grids described above. The SHAG (Small Hole Accelerator Grids) grids have an accelerator hole diameter that is  $\approx 70\%$  of the EM grids' accelerator hole diameter. This smaller hole size reduces the loss of neutral propellant. These two grid types are described in more detail in References 15 and 16. Table I shows, for example, that the 15 cm thruster with the SERT II grids was operated at one condition where the amount of current collected at the anode ( $I_{arc}$ ) was 1.7A, while the voltage difference between the anode and cathode ( $V_{arc}$ ) was 37.2 V and the ion current through the grids ( $I_{beam}$ ) was 0.258 A.

The values of the volume averaged plasma properties and the uniformity factors must be known in order to calculate the theoretical double ion density. In order to determine the values of these average

Table I  
 Thruster Sizes, Configurations and Conditions

Thruster Diameter (cm)	Grid Type	Anode Current ( $I_{arc}$ --A)	Anode Voltage ( $V_{arc}$ --V)	Ion Beam Current ( $I_{beam}$ --A)	Mass Flow Rate (A)
15.	SERT II	1.00	33.	.180	.310
15.	SERT II	1.70	37.2	.258	.307
15.	SERT II	2.05	42.6	.272	.308
15.	Dished	3.02	32.2	.499	.735
15.	Dished	4.06	37.5	.654	.725
15.	Dished	4.13	40.4	.622	.650
30.	EM	5.0	37.	1.0	1.25
30.	EM	7.5	37.	1.5	1.76
30.	EM	10.0	37.	2.0	2.29
30.	SHAG	9.5	30.	1.5	1.74
30.	SHAG	11.7	30.	2.0	2.30

plasma properties, the primary and Maxwellian electron densities and energies must be determined everywhere in the discharge chamber. The plasma properties at some point in the plasma can be measured using a Langmuir probe and analyzed using the procedure described in Reference 17. The plasma properties at sixteen different points in the plasma were measured, for each 15 cm thruster condition listed in Table I, using the movable Langmuir probe and associated circuitry described in Reference 18. The results of a typical survey (15 cm thruster - SERT II grids -37 V anode voltage) are plotted in Figure 4. This figure shows the spatial variation of the Maxwellian electron temperature, primary electron energy and the primary and Maxwellian electron densities in the discharge chamber. The Maxwellian electron temperature is seen to average approximately 9 eV over the primary electron region defined by the critical field line while the primary electron energy averages about 30 eV. The average Maxwellian electron density is about  $10^{11} \text{cm}^{-3}$  while the average primary electron density is approximately  $10^{10} \text{cm}^{-3}$  over the same region. The electron densities and energies are seen to be fairly uniform in the primary electron region but drop off rapidly outside this region. Using data similar to that plotted in Figure 4, Equations (10)-(15) and (21) were evaluated numerically by the computer program "PROP" (listed in Appendix B) to obtain the volume averaged properties and uniformity factors for each case. The results are listed in Table II along with the volume-to-surface area ratio of the primary electron region ( $V/A$ ) and the thruster operating specifications which are reproduced from Table I. The average values which resulted from an examination of Figure 4 ( $T_{\text{mx}} = 9 \text{ eV}$ ,  $\epsilon_{\text{pr}} = 30 \text{ eV}$ ,  $n_{\text{mx}} = 10^{11} \text{cm}^{-3}$ ,  $n_{\text{pr}} = 10^{10} \text{cm}^{-3}$ ) are seen to



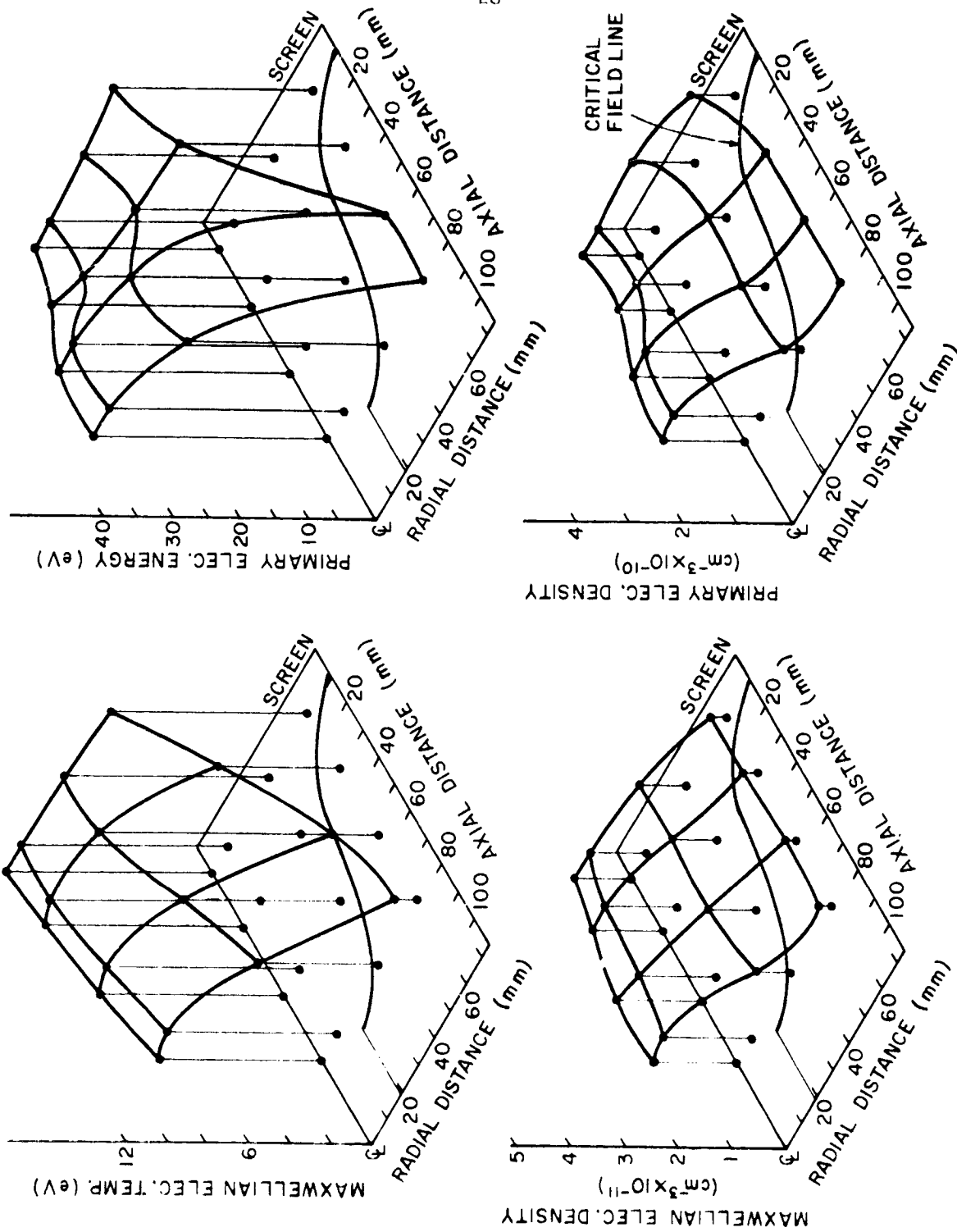


Figure 4 Plasma Property Profiles, 15 cm Thruster -  
SRT II Grids - 37 V Anode Voltage

Table II  
Experimental Results

Operating Variables	15.				15.				30.			
	15.				15.				30.			
Thrust Diameter (cm)	15.				15.				30.			
Grid Type	SERT II				HIGH PERVEANCE DISHED				EM			
Anode Current ( $I_{arc}$ ---A)	1.0	1.7	2.05		3.02	4.06	4.13		5.0	7.5	10.0	
Anode Voltage ( $V_{arc}$ ---V)	33.	37.2	42.6		32.2	37.5	40.4		37.	37.	37.	
Beam Current ( $I_{beam}$ ---A)	.190	.258	.272		.499	.654	.622		1.0	1.5	2.0	
Mass Flow Rate (A)	.310	.307	.308		.735	.725	.650		1.25	1.76	2.29	
Plasma Volume to Surface Area Ratio ( $V/A$ ---cm)	1.4	1.4	1.4		1.4	1.4	1.4		2.5	2.5	2.5	
Average Maxwellian Electron Temperature ( $T_{ex}$ ---eV)	4.2	9.1	12.2		4.3	7.1	10.2		3.3	3.6	3.8	
Average Primary-to-Maxwellian Electron Density Ratio ( $n_p/n_{mx}$ )	.034	.033	.166		.017	.042	.134		.50	.35	.25	
Average Primary Electron Energy ( $E_{pr}$ ---eV)	27.5	29.6	38.4		21.5	23.4	31.0		25.4	25.5	27.2	
Average Electron Density ( $n_e \times 10^{-10} \text{ cm}^{-3}$ )	9.80	9.10	8.07		36.0	24.3	18.2		7.51	8.97	16.4	
Uniformity Factor $F_+$	2.3	2.1	2.3		2.0	1.9	1.8		1.5	1.5	1.5	
Uniformity Factor $F_{++}$	3.1	2.5	2.6		2.5	2.1	2.0		1.8	1.9	1.8	
Measured Double-to-Single Ion Current Ratio ( $I^{++}/I^+$ )	.024	.073	.12		.036	.081	.18		.080	.125	.167	

agree well with the volume averaged values listed in Table II ( $T_{\text{max}}^* = 9.1$  eV,  $\phi_{\text{pr}}^* = 29.6$  eV,  $n_{\text{max}}^* = 8.4 \times 10^{19} \text{ cm}^{-3}$ ,  $n_{\text{pr}}^* = 7.0 \times 10^{19} \text{ cm}^{-3}$ ).  $F_+$  and  $F_{++}$ , which are defined as the ratio of the volume average ion flux to the average flux at the surface of the primary electron region, are seen to have values of 2.1 and 2.5 respectively for the case being discussed. The average plasma properties listed in Table II are observed to cover a wide range in plasma conditions; a situation which is desirable for verification of the model.

The double ion density inside the discharge chamber must also be determined. This can be accomplished indirectly by determining the double-to-single ion density ratio ( $n_{++}/n_+$ ) in the discharge chamber and the single ion density. The single ion density can be determined with sufficient accuracy by equating the single ion density to the electron density. The value of the double-to-single ion density ratio can be determined from measurements of the ratio of the double ion current to the single ion current in the exhaust beam ( $I^{++}/I^+$ ), and the equation

$$n_{++}/n_+ = \frac{I^{++}}{I^+ \sqrt{2}} \quad (31)$$

The quantity  $\sqrt{2}$  accounts for charge and Bohm criterion velocity differences between double and single ions.

The quantity " $I^{++}/I^+$ " was measured using a mass spectrometer.<sup>(19)</sup> The methods used for data acquisition and analysis using such a device are described in Reference 20 for the 15 cm thruster data and in Reference 19 for the 30 cm thruster. The results obtained are listed in the last row of Table II. They show, for example, a double-to-single ion current ratio of 2.3 for the 15 cm thruster - NEPT II grid - 37 V

anode voltage case. The general trend observed from these data is that an increase in power input ( $I_{\text{arc}}$  times  $V_{\text{arc}}$ ) for a certain thruster configuration results in an increase in the ratio  $I^{++}/I^{+}$ .

## RESULTS AND DISCUSSION

The values of the average plasma properties, listed in Table II, are observed to vary over large ranges. For example, the average Maxwellian electron temperature ranges from a low value of 3.3 eV to a high value of 12.2. Similarly the average primary-to-Maxwellian electron density ratio varies from 0.02 to 0.50. This large variation is considered sufficient to allow a general decision to be made about the accuracy of the model. Comparisons of the experimental and theoretical values of the double-to-single ion density ratio have been used to verify the model's accuracy because this quantity ( $n_{++}/n_{+}$ ) was determined experimentally. The theoretical and experimental values of the double-to-single ion density ratio are plotted as a function of propellant utilization in Figures 5 and 6. The curves labeled "THEORETICAL" result from predictions made by the model using the "Input Parameters" listed in Table II. The curves labeled "EXPERIMENTAL" result from measurements of the ratio  $I^{++}/I^{+}$  made using the mass spectrometer. The trends exhibited by the THEORETICAL and EXPERIMENTAL curves are very similar and the agreement between the THEORETICAL and EXPERIMENTAL values of the double-to-single ion density ratio is good for plasma physics work with the average error being 3%. The maximum error of 40% is observed at low double-to-single ion density ratios in the 30 cm thruster. These error values indicate the model is accurate over a wide range of plasma conditions and thruster configurations.

Since the model has been shown to be accurate in its predictions of the double-to-single ion density ratio over a wide range of conditions there is a distinct possibility that the specie densities and

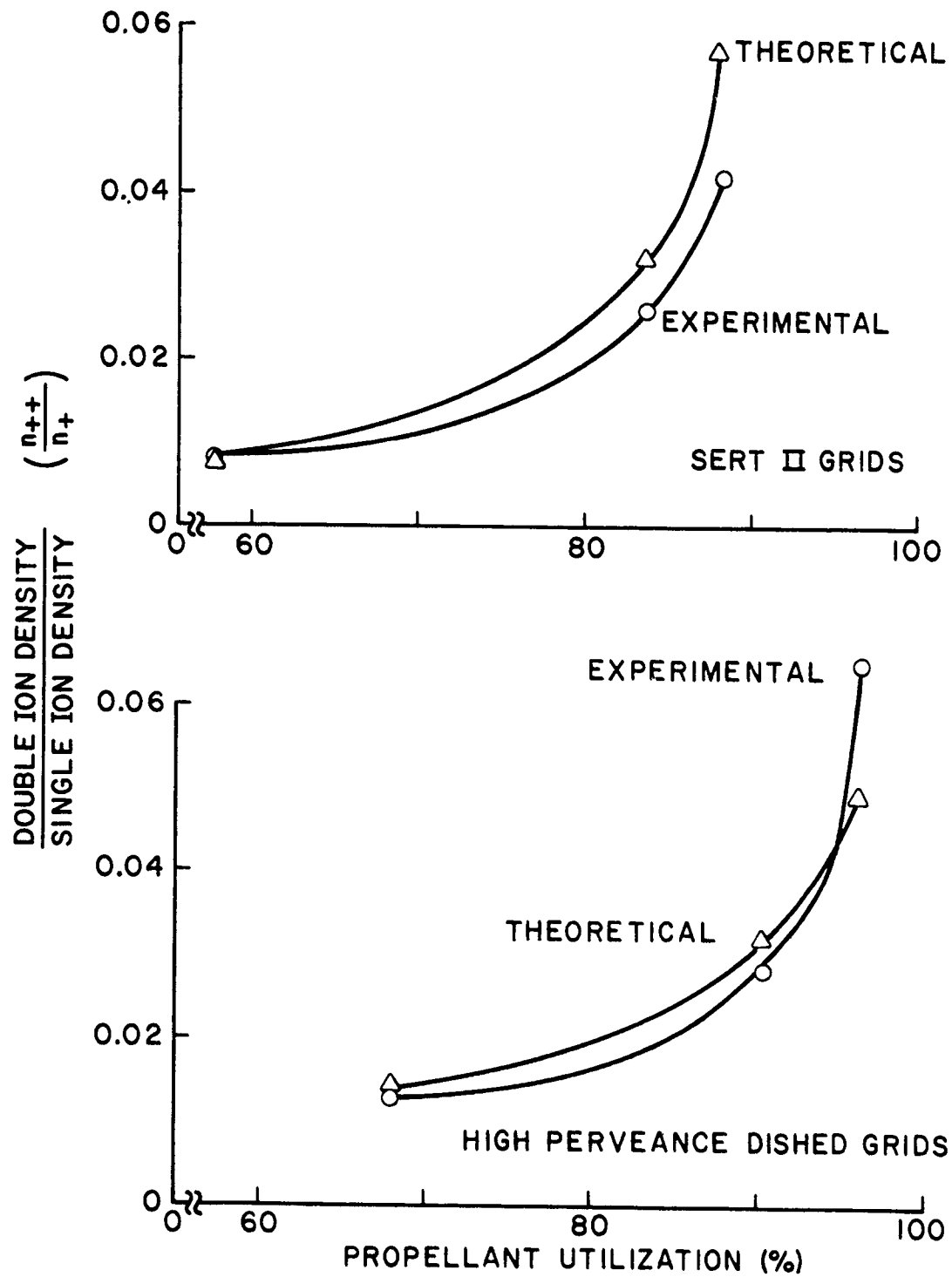


Figure 5 Double-to-Single Ion Density Ratio in a 15 cm Diameter Thruster

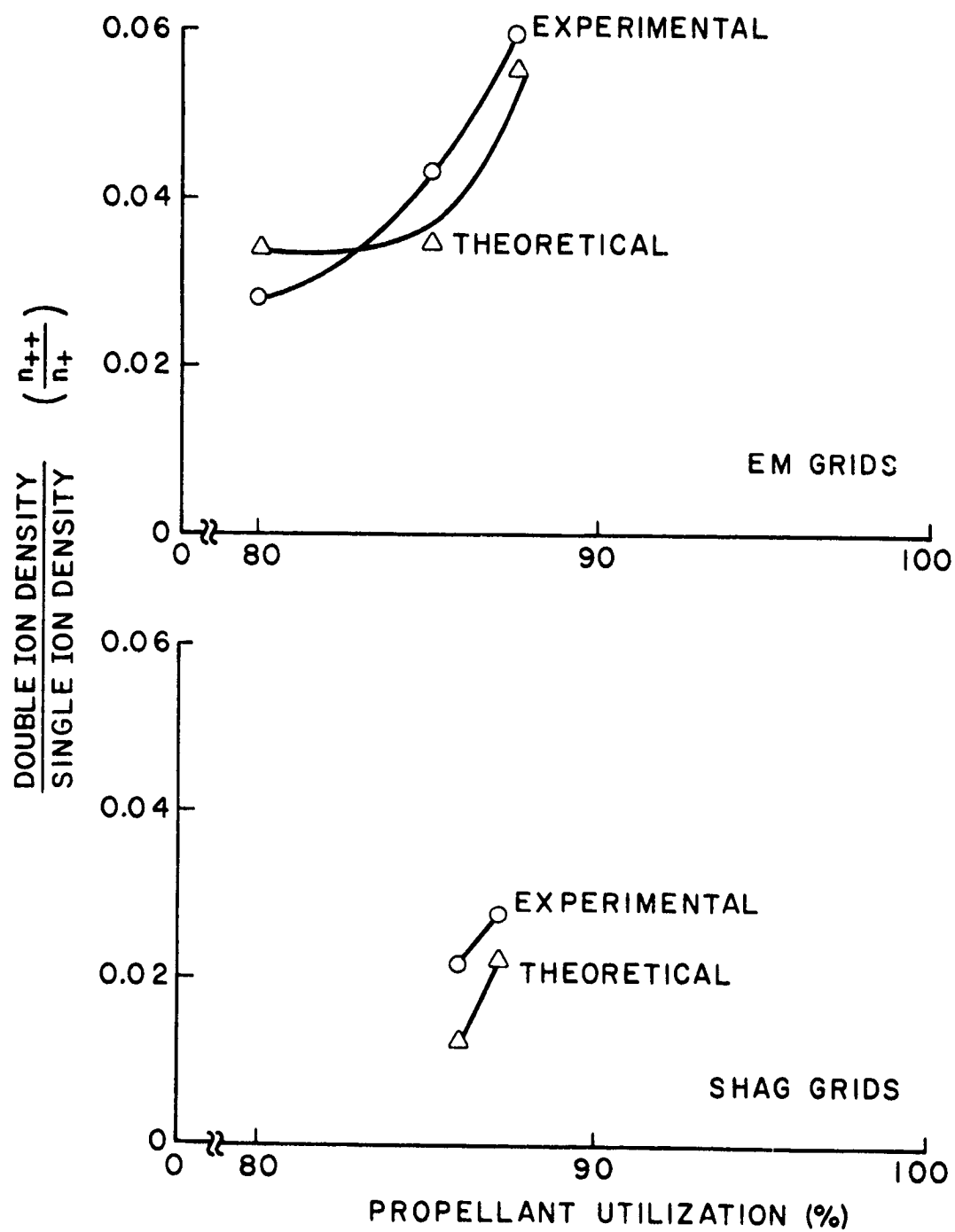


Figure 6 Double-to-Single Ion Density Ratio in a 30 cm Diameter Thruster

reaction rates used to predict the double-to-single ion density ratio are also accurate. The remainder of this section will examine the model's predictions of these specie densities and reaction rates. These quantities are listed in Table III along with the thruster operating variables and the model's input parameters which were reproduced from Table II.

The section in Table III titled "Calculated Normalized Densities" lists the model's predictions of the normalized densities of the states considered in the model where the normalized density of some specie is defined as the specie density divided by the total heavy particle density. The sum of the normalized densities for any thruster condition should therefore equal unity. Table III shows, for example, that the 15 cm diameter thruster operating with SERT II grids at 37 V anode voltage would be predicted to have 68% neutral ground state atoms, 19% neutral resonance state atoms, 6.9% singly charged ground state ions and .2% doubly charged ground state ions. The normalized density of the single ions agrees fairly well in all cases with the 10% value quoted as typical in the literature.<sup>(1)</sup> As expected the neutral ground state atoms are the most numerous.

These normalized density trends can be explained in terms of variations of plasma properties. For example, the normalized single ion density increases with increasing power input ( $I_{arc}$  times  $V_{arc}$ ) to the thruster in all cases. This occurs because an increase in the values of the volume averaged plasma properties causes the ratio of the production rate of single ions to the total neutral density to increase. The increase in the ratio indicates a smaller total neutral density is



Table III  
Predicted Densities and Reaction Rates

Operative Variables	15			15			15			15			15		
	SERT II			EDGE PLASMA II/III			IM			IM			IM		
Thruster Diameter (cm)	15	15	15	15	15	15	40	40	40	40	40	40	40	40	40
Grid Type	SERT II			EDGE PLASMA II/III			IM			IM			IM		
Anode Current ( $i_{anc}$ A)	1.5	1.7	2.0	1.5	1.7	2.0	1.5	1.7	2.0	1.5	1.7	2.0	1.5	1.7	2.0
Anode Voltage ( $V_{anc}$ V)	33	32.2	32.6	33	32.2	32.6	33	32.2	32.6	33	32.2	32.6	33	32.2	32.6
Beam Current ( $i_{beam}$ A)	180	158	171	180	158	171	180	158	171	180	158	171	180	158	171
Mass Flow Rate (A)	310	302	306	310	302	306	310	302	306	310	302	306	310	302	306
Plasma Parameters															
Plasma Volume to Surface Area Ratio (V/A-cm)	1.4	1.4	1.4	1.4	1.4	1.4	2.3	2.3	2.3	2.3	2.3	2.3	2.3	2.3	2.3
Average Maxwellian Electron Temperature ( $T_{eM}$ eV)	4.2	4.7	5.2	4.2	4.7	5.2	4.2	4.7	5.2	4.2	4.7	5.2	4.2	4.7	5.2
Average Primary-to-Maxwellian Electron Density Ratio ( $n_p^*/n_{eM}$ )	0.94	0.83	0.6	0.97	0.8	0.54	0.9	0.8	0.6	0.9	0.8	0.6	0.9	0.8	0.6
Average Primary Electron Energy ( $E_p$ eV)	27.4	29.6	30.4	27.4	29.6	30.4	27.4	29.6	30.4	27.4	29.6	30.4	27.4	29.6	30.4
Average Electron Density ( $n_e \times 10^{17}$ cm $^{-3}$ )	3.87	4.37	4.77	3.8	4.3	4.7	3.87	4.37	4.77	3.8	4.3	4.7	3.87	4.37	4.77
Uniformity Factor $f_p$	1.7	1.7	1.8	1.7	1.7	1.8	1.7	1.7	1.8	1.7	1.7	1.8	1.7	1.7	1.8
Uniformity Factor $f_{eM}$	2.7	2.7	2.8	2.7	2.7	2.8	2.7	2.7	2.8	2.7	2.7	2.8	2.7	2.7	2.8
Ion Parameters															
Measured Double-to-Single Ion Current Ratio ( $I_{d/s}$ )	0.4	0.5	0.7	0.4	0.5	0.7	0.4	0.5	0.7	0.4	0.5	0.7	0.4	0.5	0.7
Calculated Normalized Densities															
Neutral Ground State Atoms	6.5	6.8	7.1	6.5	6.8	7.1	6.5	6.8	7.1	6.5	6.8	7.1	6.5	6.8	7.1
Neutral Metastable State Atoms	5.1	5.6	6.0	5.1	5.6	6.0	5.1	5.6	6.0	5.1	5.6	6.0	5.1	5.6	6.0
Neutral Resonance State Atoms	1.7	1.9	2.1	1.7	1.9	2.1	1.7	1.9	2.1	1.7	1.9	2.1	1.7	1.9	2.1
Singly Charged Ground State Ions	7.6	7.8	8.0	7.6	7.8	8.0	7.6	7.8	8.0	7.6	7.8	8.0	7.6	7.8	8.0
Singly Charged Metastable Ions	7.1	7.3	7.5	7.1	7.3	7.5	7.1	7.3	7.5	7.1	7.3	7.5	7.1	7.3	7.5
Doubly Charged Ground State Ions	0.02	0.02	0.04	0.02	0.02	0.04	0.02	0.02	0.04	0.02	0.02	0.04	0.02	0.02	0.04
Calculated Products															
Neutral Ground State	4.1 $\times 10^{-14}$	4.1 $\times 10^{-14}$	4.1 $\times 10^{-14}$	4.1 $\times 10^{-14}$	4.1 $\times 10^{-14}$	4.1 $\times 10^{-14}$	4.1 $\times 10^{-14}$	4.1 $\times 10^{-14}$	4.1 $\times 10^{-14}$	4.1 $\times 10^{-14}$	4.1 $\times 10^{-14}$	4.1 $\times 10^{-14}$	4.1 $\times 10^{-14}$	4.1 $\times 10^{-14}$	4.1 $\times 10^{-14}$
Neutral Metastable States	3.4 $\times 10^{-14}$	3.4 $\times 10^{-14}$	3.4 $\times 10^{-14}$	3.4 $\times 10^{-14}$	3.4 $\times 10^{-14}$	3.4 $\times 10^{-14}$	3.4 $\times 10^{-14}$	3.4 $\times 10^{-14}$	3.4 $\times 10^{-14}$	3.4 $\times 10^{-14}$	3.4 $\times 10^{-14}$	3.4 $\times 10^{-14}$	3.4 $\times 10^{-14}$	3.4 $\times 10^{-14}$	3.4 $\times 10^{-14}$
Neutral Resonance States	1.1 $\times 10^{-14}$	1.1 $\times 10^{-14}$	1.1 $\times 10^{-14}$	1.1 $\times 10^{-14}$	1.1 $\times 10^{-14}$	1.1 $\times 10^{-14}$	1.1 $\times 10^{-14}$	1.1 $\times 10^{-14}$	1.1 $\times 10^{-14}$	1.1 $\times 10^{-14}$	1.1 $\times 10^{-14}$	1.1 $\times 10^{-14}$	1.1 $\times 10^{-14}$	1.1 $\times 10^{-14}$	1.1 $\times 10^{-14}$
Singly Charged Ground State	4.8 $\times 10^{-14}$	4.8 $\times 10^{-14}$	4.8 $\times 10^{-14}$	4.8 $\times 10^{-14}$	4.8 $\times 10^{-14}$	4.8 $\times 10^{-14}$	4.8 $\times 10^{-14}$	4.8 $\times 10^{-14}$	4.8 $\times 10^{-14}$	4.8 $\times 10^{-14}$	4.8 $\times 10^{-14}$	4.8 $\times 10^{-14}$	4.8 $\times 10^{-14}$	4.8 $\times 10^{-14}$	4.8 $\times 10^{-14}$
Singly Charged Metastable Ions	4.4 $\times 10^{-14}$	4.4 $\times 10^{-14}$	4.4 $\times 10^{-14}$	4.4 $\times 10^{-14}$	4.4 $\times 10^{-14}$	4.4 $\times 10^{-14}$	4.4 $\times 10^{-14}$	4.4 $\times 10^{-14}$	4.4 $\times 10^{-14}$	4.4 $\times 10^{-14}$	4.4 $\times 10^{-14}$	4.4 $\times 10^{-14}$	4.4 $\times 10^{-14}$	4.4 $\times 10^{-14}$	4.4 $\times 10^{-14}$

\* Numbers in parentheses are the fractions of the calculated interest from other neutral singly charged ions.

needed to maintain a specified single ion density and so the normalized single ion density increases as previously observed.

The last section in Table III shows the calculated production rates for singly and doubly charged ions through the various intermediate states. These production rates have been normalized by the total production rate of the specie indicated. The fraction of the associated interactions effected by the primary electrons is indicated in parenthesis. For example, at the 15 cm thruster's 37 V, SERT II grid operating point, 59% of the single ions are produced as a result of electron interaction with neutral ground state atoms and 28% resulted from electron bombardment of neutral resonance state atoms. The neutral ground state-to-single ionic state interactions were induced by primary electrons 23% of the time and by Maxwellian electrons the remainder (77%) of the time.

Thruster performance is determined primarily by the mechanism for the production and loss of single ions. The production of these ions is, according to this model, quite dependent on the neutral metastable and neutral resonance states which are ignored in most other analyses. The manner in which single ions are produced however differs a great deal between the two thrusters. In the 15 cm thruster most of the single ions are produced as a result of Maxwellian electron bombardment while primary electrons are unimportant because of their low densities. This indicates that for 15 cm thruster operation the primary electron region is the important reaction region because it is the region where high densities of high energy Maxwellian electrons occur. In the 30 cm thruster, however, relatively high primary electron densities exist and since the Maxwellian electron temperature is low most of the single ion

production results from primary electron bombardment. So for the 30 cm thruster the primary electron region is the important reaction region because it contains high densities of high energy primary electrons.

Table III indicates in all cases a large percentage of the double ions are produced from single ions. This is as one would expect because the minimum energy required to produce a double ion from a single ion is 18.7 eV while 29 eV is required to produce a double ion from a neutral ground state atom. As the power input to the thruster increases the number of electrons with energies greater than 29 eV increases causing the relative importance of the neutral-to-double transition to increase. The least energy is required for the production of double ions via singly ionized metastable states, but the densities of these states are so low that this production mechanism is unimportant.

## SIMPLIFIED MODEL

In the previous section it has been shown that most double ions are produced as a result of electron bombardment of single ions. In order to simplify the analysis of the "Theoretical Model" section the other intermediate states for double ion production can therefore be ignored with no significant loss in the accuracy of the double ion density calculations. In the simplified model presented here the approximation is made that the total rate of production of double ions equals the rate of production of double ions from single ions. This production rate is given by:

$$R_p^{++} \approx R_{p_+}^{++} = n_+^* [n_{pr}^* P_+^{++}(\xi_{pr}^*) + n_{mx}^* Q_+^{++}(T_{mx}^*)] \psi \quad (32)$$

The total loss rate of double ions is given by the equation

$$R_{l_{++}} = \frac{n_{++}^* v_{++}^* A}{F_{++}} \quad (33)$$

Equating the loss and production rates and then solving the resultant equation for the double ion density one obtains

$$n_{++}^* = n_+^* \frac{[n_{pr}^* P_+^{++}(\xi_{pr}^*) + n_{mx}^* Q_+^{++}(T_{mx}^*)] \psi}{\frac{v_{++}^* A}{F_{++}}} \quad (34)$$

The approximation  $n_e^* = n_+^*$  can now be used and Equation (18) can be substituted for the double ion velocity to obtain the following equation.

$$n_{++}^* = n_e^{*2} \frac{V}{A} F_{++} \frac{\left[ \frac{n_{pr}^*}{n_e^*} P_+^{++}(\epsilon_{pr}^*) + \frac{n_{mx}^*}{n_e^*} Q_+^{++}(T_{mx}^*) \right]}{[T_{mx}^* q (1 + n_{pr}^*/n_{mx}^*)/m_i]^{1/2}} \quad (35)$$

The double ion density can now be determined for a given thruster operating condition using this equation and the plots of  $P_+^{++}(\epsilon_{pr})$  and  $Q_+^{++}(T_{mx})$  found in Figure 7 if the volume averaged plasma properties and the uniformity factor  $F_{++}$  are known. This equation will consistently predict lower double ion densities than the complete model since it ignores the production of double ions from neutral states and the singly ionized metastable states, but this error should generally be small. The error will be greatest for plasmas with high energy electrons which can produce double ions directly from neutral states.

The last section of Table III can be used to determine the magnitude of this error for the 11 cases considered in this study. Since the simplified model considers only the single-to-double transition the error associated with this approximation can be determined from the listed value of the percentage of double ions produced from single ions. For example, for the 15 cm-SERT II grid - 37 V anode voltage case the percentage of double ions produced from single ions is 78%. This means that the value of the double ion density predicted by the simplified model would be 78% of that predicted by the complete model. Examination of Table III indicates the double ion densities calculated using the simplified model will agree well with the complete model's predictions for all the 30 cm thruster conditions because in these cases the percentage of double ions produced from single ions is greater than 97%.

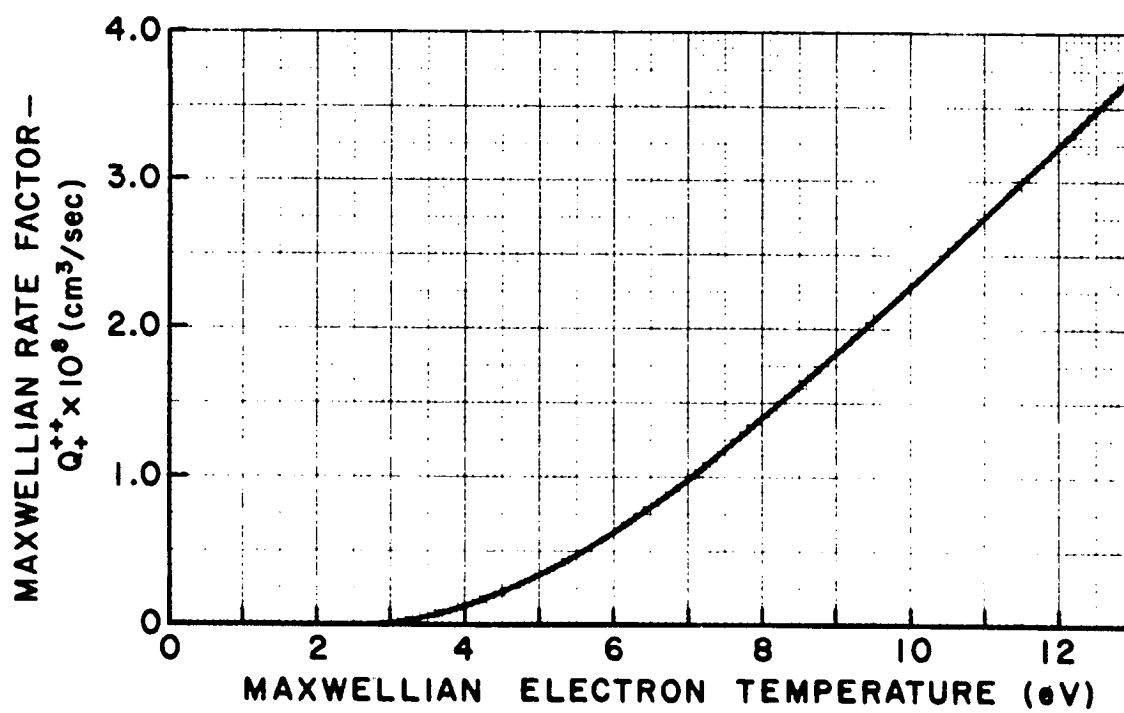
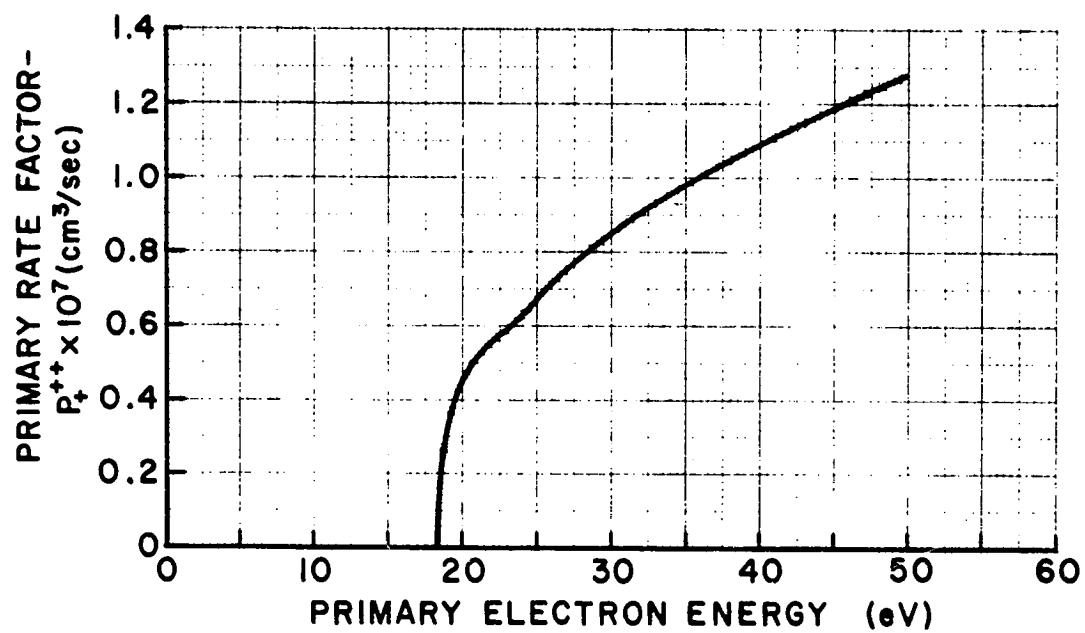


Figure 7 Rate Factors for  $\text{Hg}^+ \rightarrow \text{Hg}^{++}$

In each of these cases few electrons have energies in excess of 29 eV (the minimum energy required for the neutral-to-double transition). The simplified model will however, according to Table III, yield results which are generally low for the 15 cm thruster data (e.g. 30% low for the SERT II grid - 42 V anode voltage condition) because in these cases sufficiently high Maxwellian electron temperatures exist to cause a relatively large percentage of the electrons to have energies in excess of 29 eV.

The most accurate way to determine the values of the average plasma properties required in Equation (35) would be to conduct a Langmuir probe survey of the discharge chamber under consideration to determine the plasma properties at many different points and to then use this information in Equations (10) to (15) and (21) to determine average plasma properties. The collection of the plasma property data is however costly and time consuming. For this reason average plasma property correlations were developed. The correlating parameters used are composed of thruster operating parameters (e.g.  $I_{arc}$ ) and geometric properties (e.g.  $V/A$ ). Using the Maxwellian electron temperature data listed in Table III, for example, one obtains the correlation presented in Figure 8. The terms used in the correlating parameter are defined in Table III. The correlating parameter used in Figure 8 was determined by trial and error. The shape of a curve through the resultant data points was picked to match the trends observed in the data points. For example, the slope of the curve in the neighborhood of the low Maxwellian electron temperature points is seen to decrease. This agrees with the trend observed in the data and also agrees with a prediction, based on inelastic collision cross section data, which says a lower

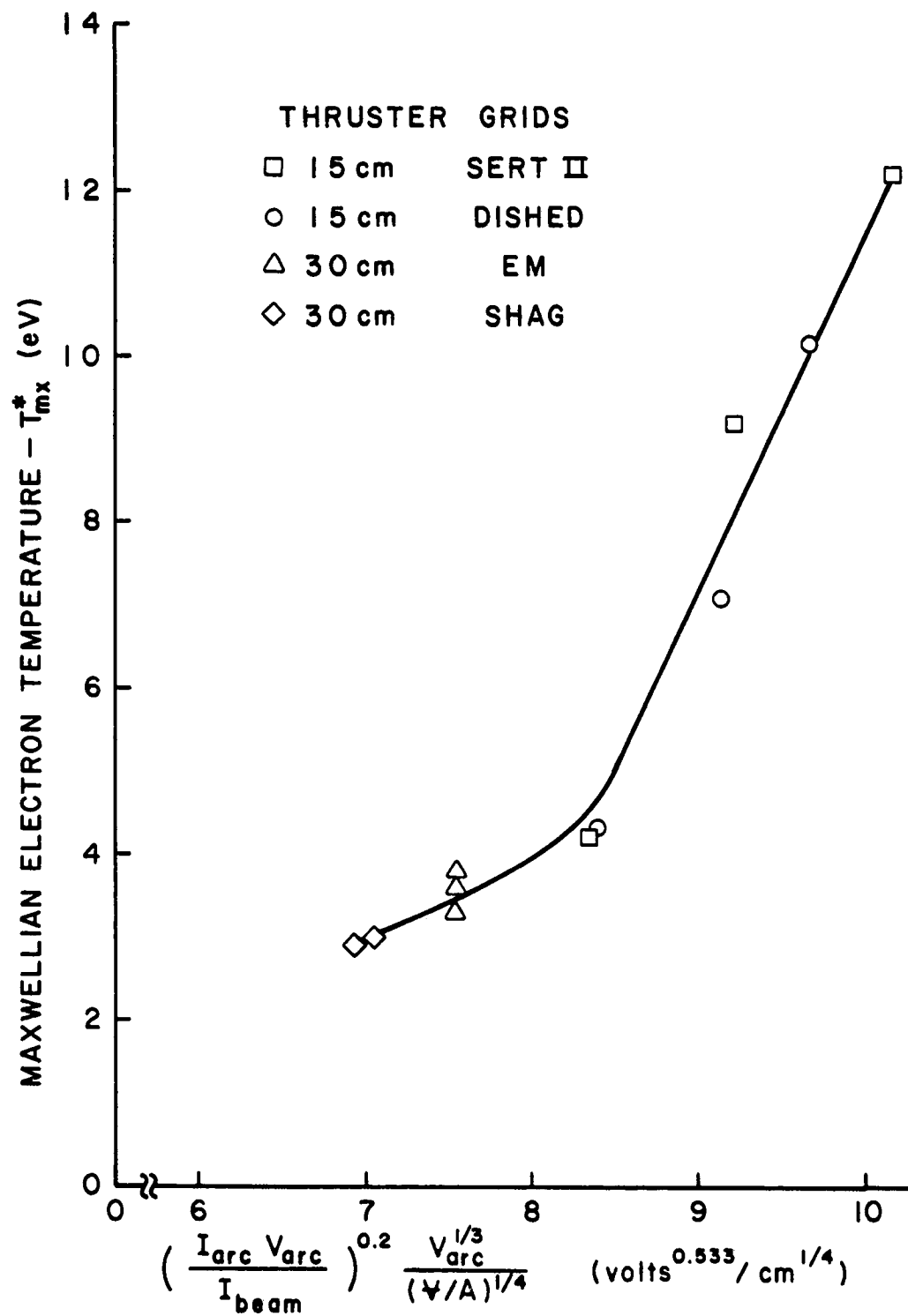


Figure 8 Maxwellian Electron Temperature Correlation



bound on the Maxwellian electron temperature should exist roughly in the neighborhood of 5 eV<sup>(1)</sup>.

The correlation for the primary electron energy is shown in Figure 9. The correlating parameter contains the quantity  $\eta_c$  which is the corrected propellant utilization. The corrected utilization was used in the correlating parameter, instead of the measured propellant utilization, because a better fit of the data points resulted from its use. The propellant utilization ( $\eta$ ) of an ion thruster depends upon the plasma properties, the effective open area for the loss of neutral atoms through the grids ( $A_0$ ) and the effective open area for the loss of ions through the grids ( $A_+$ ). The propellant utilization is defined by the equation

$$\eta = \frac{n_+ v_+ A_+}{n_+ v_+ A_+ + n_{ot} v_o A_o} \approx 1 - \frac{n_{ot} v_o A_o}{n_+ v_+ A_+} \quad (36)$$

where  $n_{ot}$  is the total neutral atom density. The primary energy (and other average plasma properties) of a given thruster correlate with the propellant utilization as defined above, but correlation between grid sets having different values of the ratio  $A_0/A_+$  is poor. The problem caused by the utilization's dependence upon grid sets can be corrected by eliminating the ratio  $A_0/A_+$  from Equation (36) and then substituting in its place the value of the ratio  $A_0/A_+$  for some standard grid set. The resultant quantity is the corrected utilization and is defined by the equation

$$\eta_c = 1 - \frac{n_{ot} v_o}{n_+ v_+} \left[ \frac{A_o}{A_+} \right]_{\text{standard}} \quad (37)$$

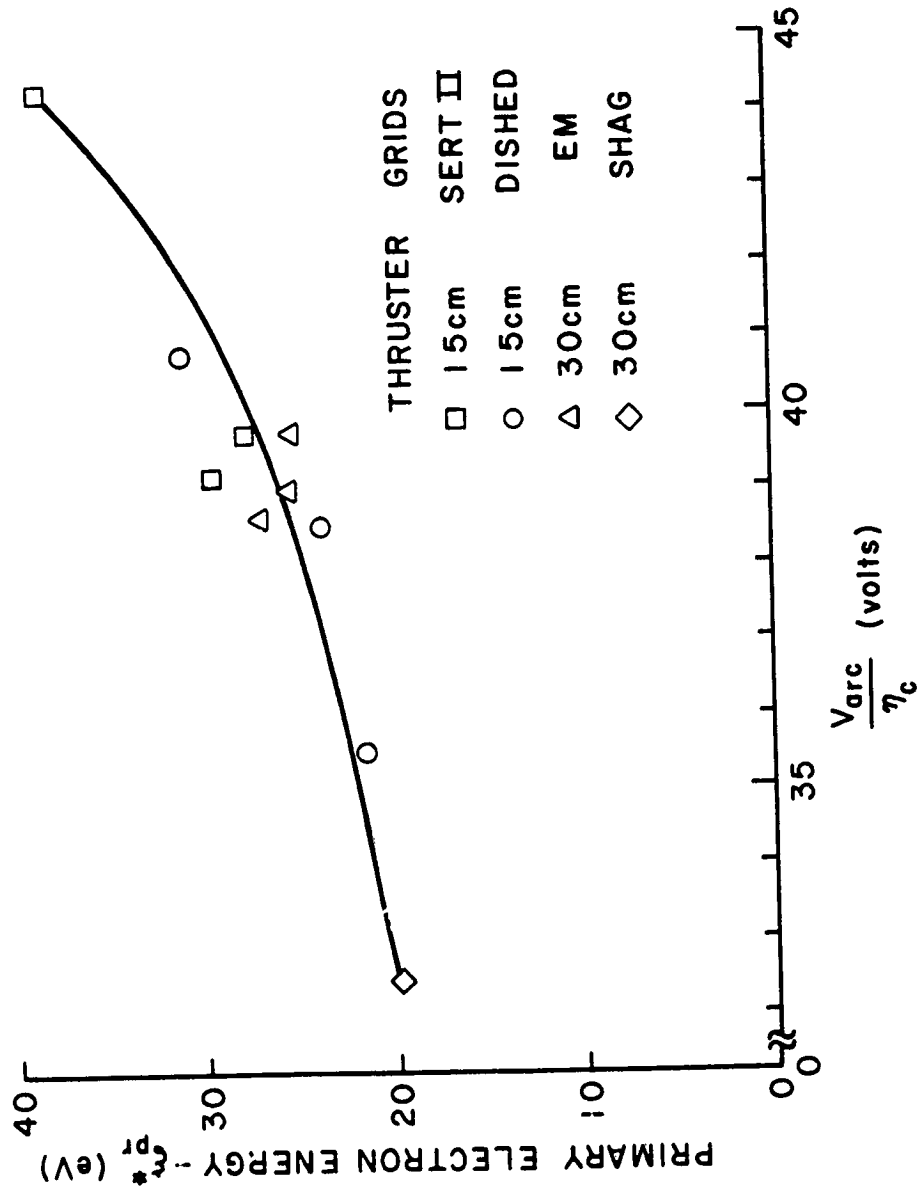


Figure 9 Primary Electron Energy Correlation

The open area for the loss of ions ( $A_+$ ) from a thruster is proportional to the open area fraction of the screen grid ( $\phi_s$ )<sup>(1)</sup>. Equilibrium flow theory<sup>(1)</sup> can be used to determine that the open area for the loss of neutral atoms ( $A_o$ ) is proportional to the quantity  $(\phi_s \phi_a)/(\phi_s + \phi_a)$  where  $\phi_a$  is the open area fraction of the accelerator grid. These two approximations can be used to define the ratio  $A_o/A_+$  as follows

$$\frac{A_o}{A_+} = \left( \frac{\phi_s \phi_a}{\phi_s + \phi_a} \right) / \phi_s = \frac{\phi_a}{\phi_s + \phi_a} \quad (38)$$

If Equations (36) - (38) are combined the following result is obtained,

$$\eta_c = 1 - .5(1 - \eta) \frac{\phi_s + \phi_a}{\phi_a} \quad (39)$$

where the constant ".5" defines  $\phi_a/(\phi_s + \phi_a)$  for the standard grid set.

Figures 10-12 show correlations for the remaining input parameters. These correlations were developed by trial and error in a manner similar to that used to obtain those in Figures 8 and 9. It should be noted that the correlation in Figure 11 is for the quantity  $n_{pr}^* [V/A]^{-1.5}$  not the primary electron density ( $n_{pr}^*$ ).

It should be understood that the correlations of Figures 8-12 are based on data obtained from strongly divergent magnetic field thrusters. The average plasma properties predicted using these figures may be inaccurate for other types of thrusters (e.g. multipole or radial field thrusters). Therefore Langmuir probe surveys should be made for these other types in order to obtain good estimates of the average plasma properties and hence accurate predictions of the double ion density.

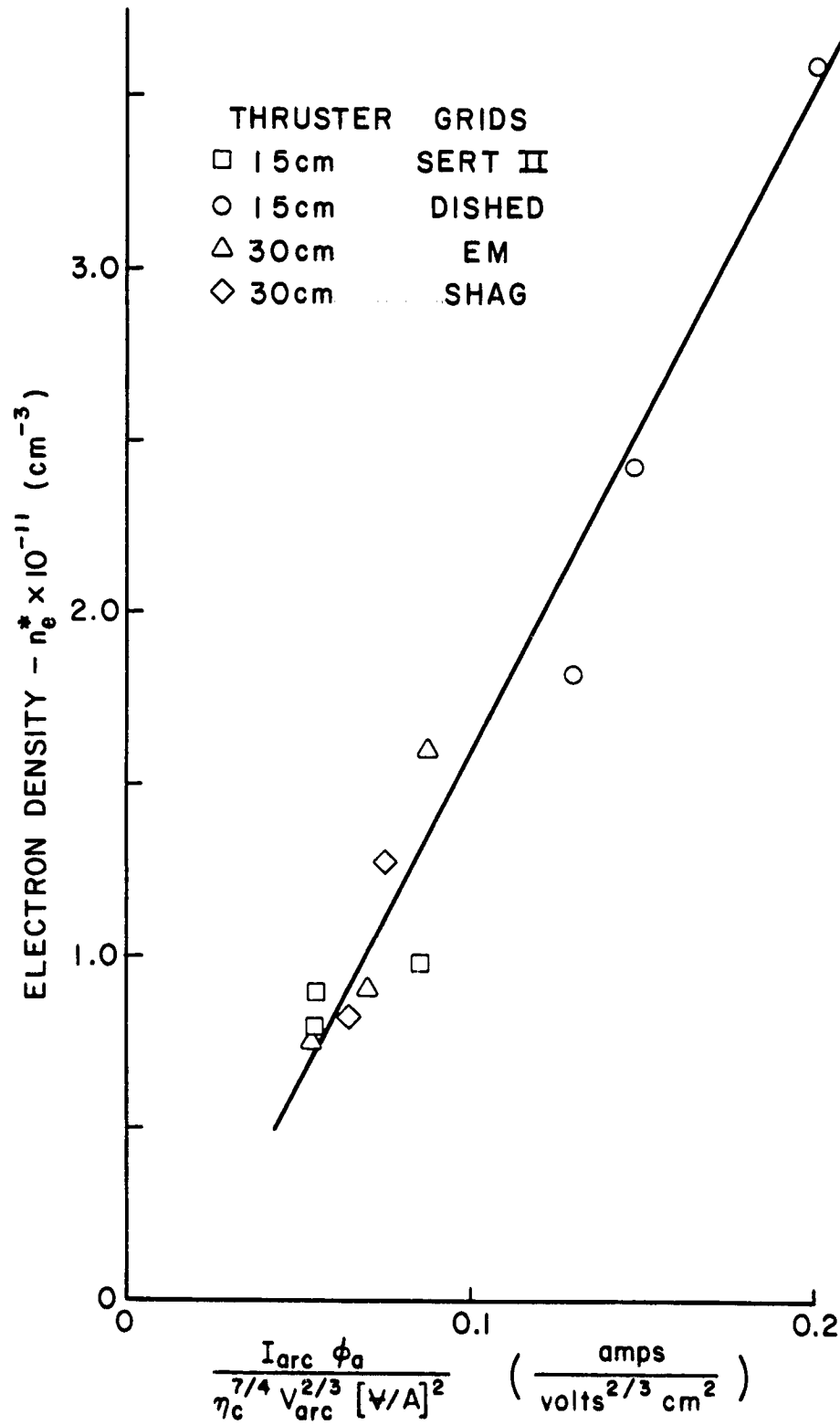


Figure 10 Electron Density Correlation

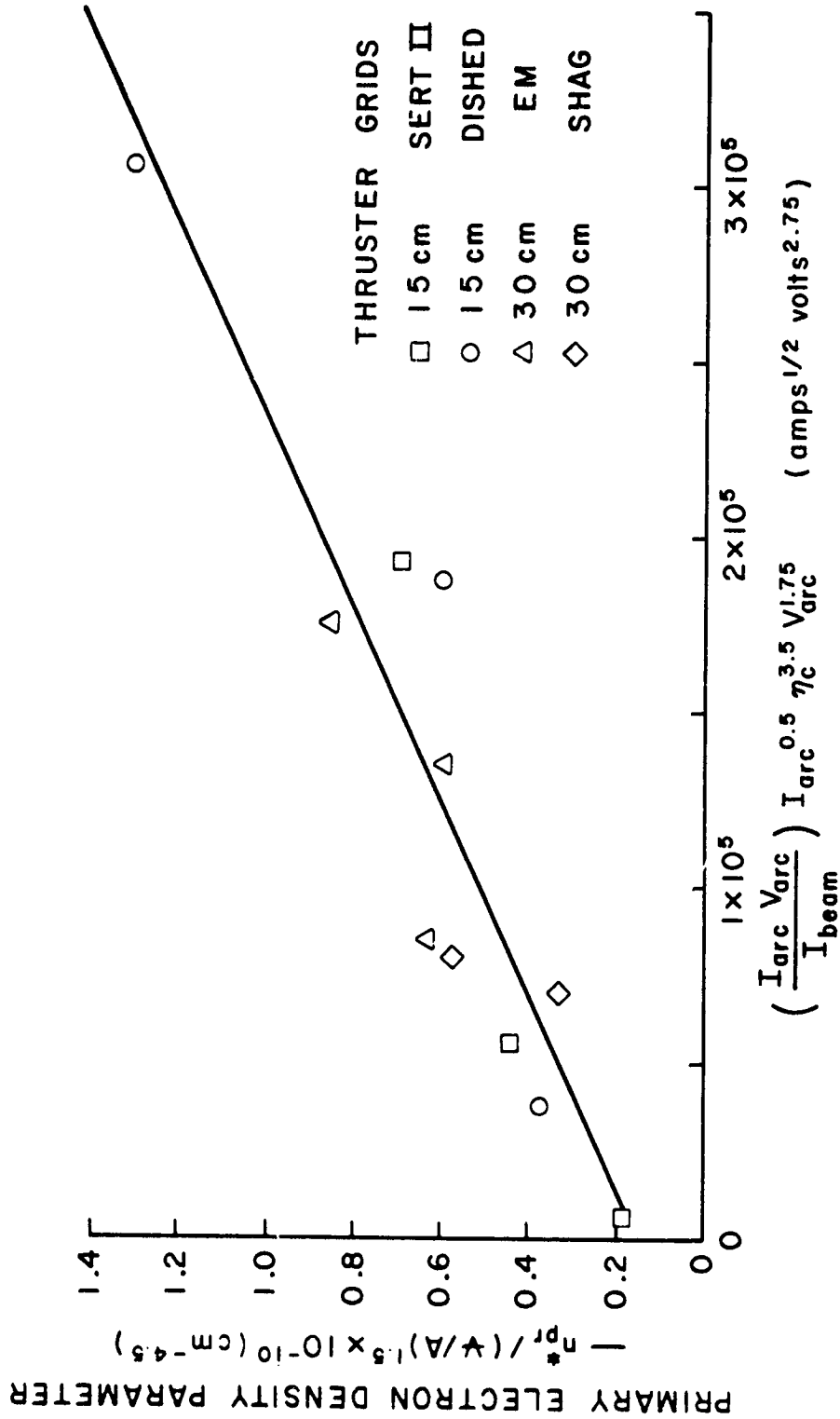
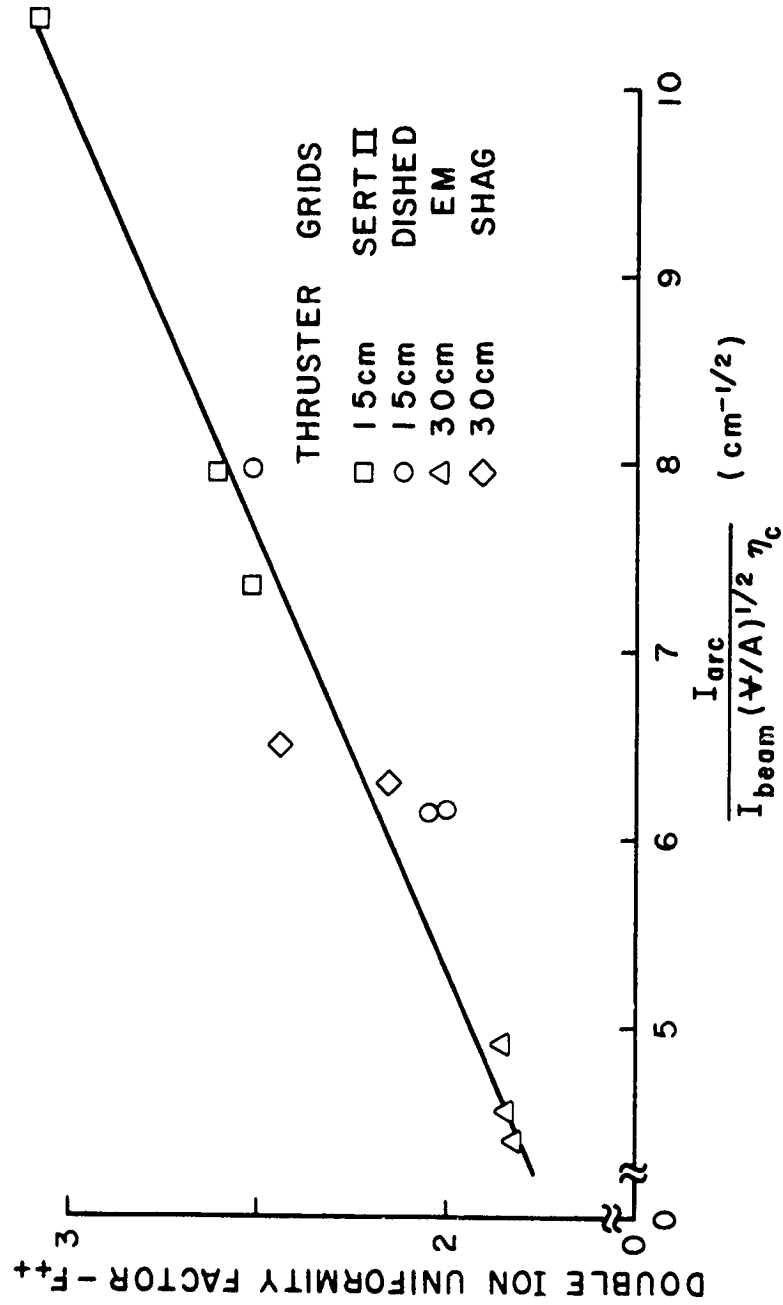


Figure 11 Primary Electron Density Correlation



Application of the simplified model can be best demonstrated through an example. Consider a 15 cm thruster operating at the conditions defined by the first section of Table IV. The corrected utilization ( $\eta_c$ ) is first calculated using Equation (39) and a value of 68% is obtained. Next the correlating parameters are calculated. For example, the value of the correlating parameter

$$\left( \frac{I_{\text{arc}} V_{\text{arc}}}{I_{\text{beam}}} \right)^{.2} V_{\text{arc}}^{1/3} (\psi/A)^{-1/4}$$

used in Figure 8 is  $8.3 \frac{\text{volts}}{\text{cm}}^{.533}$ . This value indicates the average Maxwellian electron temperature would be 4.6 eV. The remainder of the average plasma properties were determined in a similar manner. The results obtained are listed in the second section of Table IV. Using the values of the primary electron energy and the Maxwellian electron temperature one can enter Figure 7 and determine  $P_+^{++}$  (22 eV) and  $Q_+^{++}$  (4.6 eV). These quantities, together with the average densities, the uniformity factor and the volume-to-surface area ratio for this thruster are then substituted into Equation (35) to obtain the double ion density as shown in the last section of Table IV. The double ion density calculated using the simplified model is  $6.2 \times 10^{11} \text{ cm}^{-3}$  while the value calculated using the complete model is  $5.2 \times 10^{11} \text{ cm}^{-3}$ . The major reason for the discrepancy is that the electron temperature in Table IV (4.6 eV) is larger than the value used by the complete model (4.3 eV). This higher electron temperature causes  $Q_+^{++}(T_{\text{mx}}^*)$  to be too large and results in the over-estimate of the double ion density.

Table IV.

Determination of the Double Ion Density Using the Simplified Model

Measured Thruster Variables

(15 cm Thruster)

$I_{\text{arc}}$	= 3. amps	$\phi_s$	= .67
$V_{\text{arc}}$	= 32.2 volt	$\phi_a$	= .67
$I_{\text{beam}}$	= .499 amps	$\Psi/A$	= 1.4 cm
$\eta$	= .68		
$\eta_c$	= .68		

## Approximate Plasma Properties

$T_{\text{mx}}^*$	= 4.6 eV	$n_{\text{pr}}^*$	= $4.64 \times 10^9 \text{ cm}^{-3}$
$\xi_{\text{pr}}^*$	= 22. eV	$n_e^*$	= $3.51 \times 10^{11} \text{ cm}^{-3}$
$F_{++}$	= 2.55	$n_{\text{mx}}^* = n_e^* - n_{\text{pr}}^*$	= $3.46 \times 10^{11} \text{ cm}^{-3}$

## Calculation of the Double Ion Density

$$\begin{aligned}
 n_{++}^* &= \frac{(3.51 \times 10^{11} \text{ cm}^{-3})^2 (1.4 \text{ cm}) (2.55)}{\left[9.6 \times 10^9 \frac{\text{cm}^2}{\text{sec}^2 \cdot \text{eV}} (4.6 \text{ eV}) (1.013)\right]^{\frac{1}{2}}} \\
 &\times \left[.013 \left(.55 \times 10^{-7} \frac{\text{cm}^3}{\text{sec}}\right) + .987 \left(.23 \times 10^{-8} \frac{\text{cm}^3}{\text{sec}}\right)\right] \\
 &= 6.2 \times 10^9 \text{ cm}^{-3}
 \end{aligned}$$



An examination of Equation (35) will indicate some general trends which should be considered in the design and operation of electron bombardment thrusters. For example, the double ion density varies linearly with the volume-to-surface area ratio. Therefore if two thrusters have the same average plasma properties the larger thruster will have a higher double ion density. Equation (35) suggests it would be desirable to reduce the electron density since the double ion density is proportional to the square of the electron density. However, making arbitrary adjustments in the plasma properties to reduce the double ion density may have an adverse effect on other aspects of thruster performance which must also be considered. An examination of the effect of electron density on propellant utilization will indicate one of the effects such an adjustment would have. The propellant utilization previously defined in Equation (36), is reproduced below.

$$\eta = 1 - \frac{n_{ot}^* v_o A_o / A_+}{n_+^* v_+} \quad (40)$$

The single ion density ( $n_+^*$ ) can be approximated by the electron density ( $n_e^*$ ). The total neutral density ( $n_{ot}^*$ ) is the sum of the densities of all the neutral species and can be calculated using the equation

$$n_{ot}^* = n_o^* (1 + n_{mt}^* / n_o^* + n_{rt}^* / n_o^*) \quad (41)$$

where  $n_{mt}^*$  and  $n_{rt}^*$  are the total metastable and resonance states densities. The values of the ratios in Equation (41) can be calculated using equations similar in form to Equation (30). The neutral ground state density can be calculated using the equation

$$n_o^* = n_+^* (n_o^*/n_+^*) \approx n_e^* (n_o^*/n_+^*) \quad (42)$$

where the ratio  $(n_o^*/n_+^*)$  again takes a form similar to that of Equation (30). Combining these results into Equation (40) a result of the following form is obtained. "f" is a function of the Maxwellian electron temperature, primary electron energy, primary-to-Maxwellian electron density ratio and the uniformity factor  $F_+$ . The dependence of the propellant utilization on the electron density and thruster parameters is explicitly shown.

$$\eta = 1 - \frac{A_o/A_+}{n_e^* V/A} f(T_{mx}^*, \epsilon_{pr}^*, n_{pr}^*/n_{mx}^*, F_+) \quad (43)$$

One can see that a reduction in the electron density to reduce the double ion density will also have the undesirable effect of reducing the propellant utilization. However, if some changes in thruster design are made along with a reduction in the electron density the propellant utilization can be held constant while the double ion density is reduced. For example, if a new thruster were being designed one might double the volume-to-surface area ratio by making the thruster larger than its predecessor. It could then be operated at one-half the electron density of the predecessor allowing the propellant utilization to remain constant while exhibiting half the double ion density in accordance with Equation (35).

It might also be desirable to reduce the double ion density of a certain size thruster while maintaining the same propellant utilization. The propellant utilization could be held constant by reducing both the ratio  $A_o/A_+$  (which reduces the relative escape rate of neutrals) and

the electron density in a manner that keeps the ratio  $(A_0/A_+)/n_e^*$  constant. According to Equation (35) this would result in a large reduction in the double ion density which varies as the square of the electron density. The data in Table III for the two 30 cm thruster configurations at 1.5 and 2.0 amps beam current can be used to determine if theory and experiment agree for this method of double ion density reduction. The only difference in these two thruster configurations is the open area fraction of the accelerator grid. The EM accelerator grid has an open area fraction ( $\phi_a$ ) of 45% while the open area fraction for the SHAG accelerator grid is 23%. Both sets have a 69% open area fraction for the screen grid. The value of the ratio  $A_0/A_+$  can be calculated for both grid sets using Equation (38). For the EM grids the ratio  $A_0/A_+$  has a value of .39 while for the SHAG grids the value of the ratio is .25. The change from EM grids to SHAG grids then allowed operation at a given propellant utilization to occur at a lower arc voltage and hence a lower electron densities and energies and as a result lower double ion densities. In this particular case the double-to-single ion density ratios dropped from 4.4% and 6.0% to 2.2% and 2.8% respectively at two different utilizations when the SHAG grids were used. The theoretical model predicted essentially the same quantitative changes.

## CONCLUSIONS

A discharge chamber model for an electron bombardment ion thruster has been developed which considers metastable, resonance and ground state atomic and ionic production and loss mechanisms. The model can be used to predict doubly charged ion densities from plasma property information. These calculated double ion densities agree with measured values to within 40% for low values of the double-to-single ion density ratio ( $n_{++}/n_+ < 2\%$ ) and to within 20% for the rest of the data. Correlations, which relate average plasma properties to thruster operating variables such as anode current, can be used to estimate the average plasma properties in strongly divergent magnetic field thrusters when the properties themselves are not available. Singly charged ions are produced, according to this analysis, in significant numbers in two step processes through intermediate metastable and resonance states in addition to direct ionization from the neutral ground state. Doubly charged ions are produced predominantly via the singly ionized ground state with direct ground state neutral-to-double ion production becoming more significant in plasmas with high Maxwellian electron temperatures and primary electron energies. A simplified model which considers only the singly ionized ground state in double ion production can be used to predict double ion densities that agree with the complete model's predictions to within 5% when primary electron energies and Maxwellian electron temperatures are less than 29 eV and 5 eV respectively. The recent experimental observation<sup>(12)</sup> that the use of small hole accelerator grids in conjunction with lower anode voltages provides a means for reducing double ion densities in thrusters, without degrading performance, is supported by the model.

## REFERENCES

1. Kaufman, H. R., "Technology of Electron-Bombardment Ion Thrusters," Advances in Electronics and Electron Physics, Vol. 36, Academic Press, 1974.
2. Kieffer, L. J., "Electron Impact Ionization Cross Section Data for Atoms, Atomic Ions and Diatomic Molecules," Rev. Mod. Physics, Vol. 38, No. 1, pp.15, 23, 1966.
3. Shpenik, O. B. and I. P. Azpesochnyi, "Excitation Cross Sections near the Threshold for Electron Atom Collisions," Optics and Spect., Vol. 23, pp.7-10, 1967.
4. Kupriyanov, S. E. and Z. Z. Latypov, "Ionization of Positive Ions by Electrons," Soviet Physics JETP, Vol. 19, No. 3, pp. 558-559, Sept. 1964.
5. McConnell, J. C. and B. L. Moiseiwitsch, "Excitation of Mercury by Electrons," J. Phys. B., Vol. 1, No. 3, pp. 409-412.
6. Gryzinski, Michal, "Classical Theory of Atomic Collisions. I. Theory of Inelastic Collisions," Phys. Rev., Vol. 138, No. 2A, p. A341, April 19, 1965.
7. Strickfaden, W. B. and K. L. Geiler, "Probe Measurements of the Discharge in an Operating Electron Bombardment Engine," AIAA Journal, Vol. 1, No. 8, pp. 1815-1823, August 1963.
8. Masek, T. D., "Plasma Properties and Performance of Mercury Ion Thrusters," AIAA Paper No. 69-256, March 3-5, 1969.
9. Wilbur, P. J., "Hollow Cathode Restartable 15 cm Diameter Ion Thruster," NASA CR-134532, December, 1973.
10. Peters, R. R. and P. J. Wilbur, "Double Ion Production in Mercury Thrusters," AIAA Paper 75-398, March 19-21, 1975.
11. Mitchell, A. C. G., "Resonance Radiation and Excited Atoms," Cambridge at the University Press, 1961.
12. Vahrenkamp, R. P., Personal Communication, January, 1976.
13. Bechtel, R. J., Csiky, G. A., and D. C. Byers, "Performance of a 15-centimeter Diameter, Hollow Cathode Kaufman Thruster," AIAA Paper No. 68-88, January 22-24, 1968.
14. Poeschel, R. L., King, H. J., and D. E. Schneider, "An Engineering Model 30 cm Thruster," AIAA Paper No. 73-1084, Oct. 31 - Nov. 2, 1973.

15. Poeschel, R. L., et al., "2.5 Kw Advanced Technology Ion Thruster," NASA CR-134687, August, 1974.
16. Poeschel, R. L., et al., "High Power and 2.5 Kw Advanced Technology Ion Thruster," Monthly Report No. 7, Contract NAS 3-19703, January, 1976.
17. Wilbur, P. J., "15 cm Diameter Ion Thruster Research," NASA CR-134755, December, 1974.
18. Wilbur, P. J., "An Experimental Investigation of a Hollow Cathode Discharge," NASA CR-130847, December, 1971.
19. Vahrenkamp, R. P., "Measurement of Doubly Charged Ions in the Beam of a 30 cm Mercury Bombardment Thruster," AIAA Paper No. 73-1057, Oct. 31 - Nov. 2, 1973.
20. Wilbur, P. J., "15 cm Mercury Ion Thruster Research," NASA CR-134905, December, 1975.

## APPENDIX A

The computer program "HG", which can be used to predict the densities of excited atomic and ion states considered in the complete model, is listed below. The input parameters needed by this program can be approximated using the correlations in Figures 8-12. More accurate input parameters can be determined using the computer program "PROP", listed in Appendix B, and data obtained from a Langmuir probe survey of the discharge chamber. The computer program "HG" uses the equations developed in the "Theoretical Model" section and carries out the calculations in the manner suggested at the end of that section. Comment cards are included in the listing to indicate what calculations, etc. are to be carried in each section.

Values of the functions  $P_{\alpha}^Y(\epsilon_{pr})$  and  $Q_{\alpha}^Y(T_{mx})$  are listed immediately after the computer program listing. The particular initial state ( $\alpha$ ) and final state ( $\gamma$ ) are indicated in the last twenty columns. For example, the label "HGM-HG+ 3P0" indicates the initial state for the reaction is the  $6^3P_0$  metastable state and the final state is the singly ionized ground state. The first seven cards listed with a particular identifying label contain the values for  $P_{\alpha}^Y(\epsilon_{pr})$  while the second seven list values for  $Q_{\alpha}^Y(T_{mx})$ .

```

PROGRAM HG (INPUT,OUTPUT,PUNCH,TAPES=INPUT,TAPF6=OUTPUT,TAPE8=PUNCH
1H,FI,IMPL)
COMMON /A/ NP,NM,TEMP,PRINRG
COMMON /B/ UTT(4,25),PD(4,25),IK
DIMENSION A(8), R(3), C(3), D(3), F(3), SXO0M(2,2,21), SE00M(2,2,2HG
11), SX01(2,21), SE01(2,21), SX02(2,21), SE02(2,21), SX0M1(2,2,21),HG
2 SE0M1(2,2,21), SX11M(2,2,21), SE11M(2,2,21), SX12(2,21), SE12(2,2HG
31), RR(2), TR(2), SE1M2(2,2,21), RA0M0(2), RA1M0(2), SX(2,21), SF(HG
42,21), P2(8), TI(8), X(8), Y(8), G(8), R(5), Z(8), H(8), SX0R(2,2,HG
521), SE0R(2,2,21), SX11(2,2,21), SE11(2,2,21), FR(2), TM(2), W(2),HG
6 G(2), IK(2), XSM(2), XSM(2), XPSM(2), XPSMM(2), FREE(2), PHLOSS(HG
72), TAU(2), XLAM(2), OPP(6,6), XNE(6), XL(3,6,10), PNE(6,10), SP(6HG
8,6), P2A(7), HA(7), PYP(30), PNO(4), SD(14,6,10), TT1(14,8), PP(10HG
9), PR(10), FXP(30), SX1M2(2,2,21), TMP(5), QT(8), QR(8)
REAL NP,NM
DATA X(1),TTI(1,1),TTI(2,1),TTI(3,1),TTI(4,1),TTI(5,1),TTI(6,1),TTHG
11(7,1),TTI(8,1),TTI(9,1),TTI(10,1),TTI(11,1),TTI(12,1),TTI(13,1),THG
2TI(14,1),TM,TR,TK,H(1),Z(1),Z(2)/10MPRI ENERGY,10HNEUT DENS,.10HNMHG
3/NO PERC,10HNR/NO PERC,10HNR/NO PERC,10HNR/NO PERC,10HNR/NO PERC,1HG
40HNR/NOT ,10HNR/NOT ,10HREAM MA. ,10HNR CM-3 ,10HNR CM-3HG
5 ,10HI ARC AMP,.10EV/BFAMION,10H ,10H 3P0 ,10H 3PHG
62 ,10H 3P1 ,10H 1P1 ,10H 2D 5/2 ,10H 2D 3/2 ,10HGHG
7N+/N+ ,10H PLOT WITH ,10H CONSTANT/
DATA EP,TAU,XLAM/5.545,6.7,.00000010H,.000000013,.00002537,.00001HG
1849/
FR(A,B)=(A(1)*R(1)+A(2)*R(2))/(A(1)+A(2))
C
C THIS PROGRAM IS SET UP FOR MERCURY ONLY
C SET UP OF THE PROGRAM
C
NMZ=10
NNN=0
DO 101 I=2,8
H(I)=10H
101 X(I)=10H
DO 102 I=3,8
102 Z(I)=10H
DO 103 J=1,14
DO 103 I=2,8
103 TTI(J,I)=10H
DO 104 I=1,8
QT(I)=TTI(13,I)
104 QR(I)=10H
QR(1)=10HUTL.
NU=2
DO 105 I=1,3
105 A(I)=1.
C
C READ IN THE INTEGRATED CROSS SECTIONS
C 1 -- INDICATES DATA FOR PRIMARY ELECTRONS
C 2--- INDICATES DATA FOR MAXWELLIAN ELECTRONS
C
C NEUTRAL TO SINGLE
C
C READ (5,168) ((SF01(J,I),SX01(J,I),I=1,21),J=1,2)
C
C NEUTRAL TO DOUBLE
C
C READ (5,168) ((SF02(J,I),SX02(J,I),I=1,21),J=1,2)
C
C SINGLE TO DOUBLE
C
C READ (5,168) ((SF12(J,I),SX12(J,I),I=1,21),J=1,2)
C
C NEUTRAL TO METASTABLE

```



C	READ (5,168) (((SE00M(I,J,K),SX00M(I,J,K),K=1,21),J=1,2),I=1,2)	HG	560
C	NEUTRAL TO RESONANCE	HG	670
C		HG	680
C	READ (5,168) (((SE01(I,J,K),SX01(I,J,K),K=1,21),J=1,2),I=1,2)	HG	690
C	METASTABLE ATOM TO SINGLE	HG	700
C		HG	710
C	READ (5,168) (((SE02(I,J,K),SX02(I,J,K),K=1,21),J=1,2),I=1,2)	HG	720
C	SINGLE METASTABLE TO DOUBLE	HG	730
C		HG	740
C	READ (5,168) (((SE03(I,J,K),SX03(I,J,K),K=1,21),J=1,2),I=1,2)	HG	750
C		HG	760
C	SINGLE METASTABLE TO DOUBLE	HG	770
C		HG	780
C	READ (5,168) (((SE11M(I,J,K),SX11M(I,J,K),K=1,21),J=1,2),I=1,2)	HG	790
C	RESONANCE TO SINGLE	HG	800
C		HG	810
C	READ (5,168) (((SE11(I,J,K),SX11(I,J,K),K=1,21),J=1,2),I=1,2)	HG	820
C	SINGLE TO SINGLE METASTABLE	HG	830
C		HG	840
C	READ (5,168) (((SE11M(I,J,K),SX11M(I,J,K),K=1,21),J=1,2),I=1,2)	HG	850
C		HG	860
C	READ IN DATA	HG	870
C	ND=NO. OF DIFFERENT PRIMARY ENERGIES DESIRED FOR EACH ELECTRON DENS	HG	880
C	DP=(RFLW) DELTA PRIMARY ENERGY	HG	890
C	NS=NO. OF DIFFERENT ELECTRON DENSITIES USED PER RUN	HG	900
C	NRR=NO. OF RUNS	HG	910
C	IFLAG=1 NO INTERPOLATION FOR MASS FLOW RATE	HG	920
C		HG	930
C	READ (5,142) ND,NS,NRR,IFLAG	HG	940
C		HG	950
C	BEGIN THE RUNS	HG	960
C		HG	970
C	DP=10.	HG	980
C	DO 134 IP=1,NRR	HG	990
C		HG	1000
C	EQUIVALENT OPEN AREA FOR NEUTRALS AND CHARGED PARTICLES. VOLUME OF	HG	1010
C	PRIMARY ELECTRON REGION. NONUNIFORMITY PARAMETERS.	HG	1020
C		HG	1030
C	READ (5,141) OPN,OPC,VOL,F1,F2	HG	1040
C		HG	1050
C	NO. OF DIFFERENT MASS FLOW RATES DESIRED	HG	1060
C		HG	1070
C	NC=2	HG	1080
C		HG	1090
C	VALUES OF M	HG	1100
C		HG	1110
C	IF (IFLAG.EQ.1) GO TO 106	HG	1120
C	READ (5,141) (P10(I),I=1,NC)	HG	1130
106	KKK=1	HG	1140
	XNI=.05	HG	1150
	DO 126 J=KKK,NS	HG	1160
	DP=J,DP=15.	HG	1170
	XN1=.05	HG	1180
	XN2=0.	HG	1190
	XN3=0.	HG	1200
	XN4=0.	HG	1210
C	PRIMARY ELECTRON VOLUME TO AREA, AREA, TEMPERATURE, DENSITY, PRIMARY	HG	1220
C	MAXWELLIAN RATIO, ELECTRON DENSITY.	HG	1230
C		HG	1240
C	IF (IFLAG.EQ.1) GO TO 107	HG	1250
C	READ (5,142) A,TEMP,DUMMY,TEMPOR,TEMPNS	HG	1260
C	IF (IFLAG.EQ.1) GO TO 107	HG	1270
C	IF (IFLAG.EQ.1) GO TO 107	HG	1280
C	IF (IFLAG.EQ.1) GO TO 107	HG	1290
C		HG	1300
C		HG	1310

C	ELECTRON DENSITIES FOR ITERATION ON MASS FLOW RATE	HG	1320
C		HG	1330
	READ (5,140) (TMP(L),L=1,NS)	HG	1340
	GO TO 109	HG	1350
107	ELDENS=TMP(JJ)	HG	1360
	GO TO 109	HG	1370
108	WRITE (6,139)	HG	1380
109	CONTINUE	HG	1390
	XNF(JJ)=ELDENS	HG	1400
	ELD=ELDENS/1.F18	HG	1410
	ENCODE (64,144,II) VA,ELD,TEMP,DENR	HG	1420
	DO 128 II=1,ND	HG	1430
	SEV=0.	HG	1440
	WRITE (6,145) VA,ELDENS,TEMP,PRINPS,DENR	HG	1450
	WRITE (6,146) VOL,OPN,OPC,F1,F2	HG	1460
	TOT=1.+1./DENR	HG	1470
	NP=ELDENS/TOT	HG	1480
	NM=ELDENS/TOT/DENR	HG	1490
	FFNL=20.*TEMP	HG	1500
	CALL YINTEG (SX02,SE02,1.,SUMM,PRSUM)	HG	1510
		HG	1520
C	CALCULATION OF METASTABLE/ NEUTRAL GROUND STATE RATIO	HG	1530
C		HG	1540
C		HG	1550
	DO 112 J=1,2	HG	1560
	DO 110 I=1,2	HG	1570
	DO 110 K=1,21	HG	1580
	SX(I,K)=SX00M(J,I,K)	HG	1590
110	SE(I,K)=SE00M(J,I,K)	HG	1600
	CALL YINTEG (SX,SE,1.,SUM,PRSUM)	HG	1610
	DO 111 I=1,2	HG	1620
	DO 111 K=1,21	HG	1630
	SX(I,K)=SX0M1(J,I,K)	HG	1640
111	SE(I,K)=SE0M1(J,I,K)	HG	1650
	CALL YINTEG (SX,SE,1.,SUM2,PRSUM2)	HG	1660
	WLOSS=236./VA/4.	HG	1670
	WALL=WLOSS	HG	1680
	RA0M0(J)=SUM/(WLOSS+SUM2+SUMM)	HG	1690
	WRITE (6,147) TM(J),RA0M0(J)	HG	1700
	WRITE (6,161)	HG	1710
	WRITE (6,163) SUM,PRSUM	HG	1720
	SEV=SEV+SUM*PRSUM	HG	1730
	WRITE (6,162)	HG	1740
	WRITE (6,167) WLOSS,SUM2,PRSUM2,SUMM,PRSUMM	HG	1750
	TI=WLOSS+SUM2+SUMM	HG	1760
	AA=WLOSS/II	HG	1770
	AB=SUM2/II	HG	1780
	AC=SUMM/II	HG	1790
	WRITE (6,148) AA,AB,AC	HG	1800
112	CONTINUE	HG	1810
	SD(2,JJ,II)=(RA0M0(1)+RA0M0(2))*100.	HG	1820
C		HG	1830
C	CALCULATION AND ITERATION FOR RESONANCE/NEUTRAL, SINGLE/NEUTRAL,	HG	1840
C	NEUTRAL DENSITY	HG	1850
C		HG	1860
	JML=-1	HG	1870
	IFLAG=0	HG	1880
	I2=II-2	HG	1890
	I1=II-1	HG	1900
	IF (II.GT.2) XN1=(2.*SD(4,JJ,I1)-SD(4,JJ,I2))/100.	HG	1910
	XN1=XN1+XNM+XN2	HG	1920
	XSM(2)=0.	HG	1930
C		HG	1940
C	GUESS NEUTRAL DENSITY	HG	1950
C		HG	1960
113	XN0=ELDENS/II/1000000.	HG	1970
C		HG	

```

C      CALCULATE RESONANCE/NEUTRAL RATIO
C
      DO 117 J=1,NQ
      IF (IFLAG.EQ.1) GO TO 116
      DO 114 I=1,2
      DO 114 K=1,21
        SX(I,K)=SXOR(J,I,K)
114      SE(I,K)=SEOR(J,I,K)
        CALL YINTEG (SX,SE,1.,XSM(J),XPSM(J))
      DO 115 I=1,2
      DO 115 K=1,21
        SX(I,K)=SXR1(J,I,K)
115      SE(I,K)=SER1(J,I,K)
        CALL YINTEG (SX,SE,1.,XSM(J),XPSM(J))
116      CONTINUE
      DVD=33963./XLAM(J)
      SIGMAC=.112/DVD*XLAM(J)**2/TAU(J)
      FRF(J)=1./(XND*SIGMAC)
      PHLOSS(J)=1./(9.E12*VA*(TAU(J)*XND*SIGMAC)**2)
117      RR(J)=XSM(J)/(WALL+PHLOSS(J)+XSM(J)+SUMM)
      IF (IFLAG.EQ.1) GO TO 118
      CALL YINTEG (SX01,SE01,1.,SUM1,PRSUM1)
      CALL SUMIT (SX01,SE01,2.,RABNO,TSUM1,R,C)
      Q(2)=0.
      Q(2)=0.
118      CALL SUMIT (SXR1,SER1,NQ,RR,TSS,W,Q)
      IF (IFLAG.EQ.1) GO TO 119
C
C      CALCULATION OF SINGLE/NEUTRAL RATIO
C
      VP=SQRT(TEMP*4.R038E9*(1.+NP/NM))/100.
      WLOSS=VP/VA/F1
      CALL SUMIT (SX11M,SE11M,2.,A,TSUM2,D,E)
      CALL YINTEG (SX12,SE12,1.,SUM2,PRSUM2)
119      RNIO=(SUM1+TSUM1+TSS)/(WLOSS+TSUM2+SUM2)
C
C      CHECK OF ERROR IN GUESS OF NEUTRAL DENSITY
C
      RNPO=RNIO*XN2+XNM
      FRF0R=ARS((RNPO-XN1)/RNPO)
      XN1=RNIO+XN2+XNM
      XN1=RNIO
      JKL=JKL+1
      IFLAG=1
      IF (ERROR.GT..03) GO TO 113
C
C      NEUTRAL GROUND STATE ATOM DENSITY
C
      XND=FDENS/XN1/1000000.
      WRITE (6,144) XND,JKL
      SD(3,JJ,II)=(R+(1)+RR(2))*100.
      SD(1,JJ,II)=XND
      SD(4,JJ,II)=RNIO*100.
      XKA=100./(100.+SD(3,JJ,II)+SD(2,JJ,II))
      SD(7,JJ,II)=RNIO*XKA
      XN1=XND*(1.+XND*(1)+RABNO(2)+R(1)+RR(2))
      XL(1,JJ,II)=XN1*5750.
C
C      PRINT OUT RESONANCE ATOM DENSITY RATIO
C
      DO 120 J=1,NQ
      WRITE (6,145) FR(J),R+(J),FRF(J)
      WRITE (6,146)
      WRITE (6,147) XSM(J),XPSM(J)
      WRITE (6,148)
      WRITE (6,149)
      WRITE (6,150)
      WRITE (6,151)
      WRITE (6,152)

```

```

1      WRITE (6,152) WALL,PHLOSS(J),XSM(J),XPSMM(J),SUMM,PRSHG 2640
      UNM  HG 2650
      TT=WALL+PHLOSS(J)+XSM(J)+SUMM  HG 2660
      AA=WALL/TT  HG 2670
      AH=XSM(J)/TT  HG 2680
      AC=SUMM/TT  HG 2690
      AD=PHLOSS(J)/TT  HG 2700
      WRITE (6,151) AA,AD,AH,AC  HG 2710
120    CONTINUE  HG 2720
C      PRINT OUT SINGLE ION DENSITY RATIO  HG 2730
C      HG 2740
C      HG 2750
      WRITE (6,153) RNIO  HG 2760
      SD(10,J,J,11)=RNIO*XNO  HG 2770
      PRIF=FR(B,C)  HG 2780
      WRITE (6,161)  HG 2790
      PRIG=FR(W,D)  HG 2800
      PRIH=FR(D,E)  HG 2810
      WRITE (6,164) SUM1,PRSUM1,TSUM1,PRIF,TSS,PRIG  HG 2820
      SEV=SEV+SUM1*PRSUM1+TSUM1*PRIF+TSS*PRIG  HG 2830
      TT=SUM1+TSUM1+TSS  HG 2840
      AA=SUM1/TT  HG 2850
      AR=TSUM1/TT  HG 2860
      AC=TSS/TT  HG 2870
      WRITE (6,154) AA,AH,AC  HG 2880
      WRITE (6,162)  HG 2890
      WRITE (6,167) WLOSS,SUM2,PRSUM2,TSUM2,PRIH  HG 2900
      TT=SUM2+WLOSS+TSUM2  HG 2910
      AA=WLOSS/TT  HG 2920
      AR=SUM2/TT  HG 2930
      AC=TSUM2/TT  HG 2940
      WRITE (6,148) AA,AH,AC  HG 2950
C      CALCULATION OF SINGLE META/NEUTRAL RATIO  HG 2960
C      HG 2970
C      HG 2980
C      HG 2990
      DO 123 J=1,2  HG 3000
      DO 121 I=1,2  HG 3010
      DO 121 K=1,21  HG 3020
      SX(I,K)=SX11M(J,I,K)  HG 3030
121    SE(I,K)=SE11M(J,I,K)  HG 3040
      CALL YINTEG (SX,SE,RNIO,SUM1,PRSUM1)  HG 3050
      DO 122 I=1,2  HG 3060
      DO 122 K=1,21  HG 3070
      SX(I,K)=SX1M2(J,I,K)  HG 3080
122    SE(I,K)=SE1M2(J,I,K)  HG 3090
      CALL YINTEG (SX,SE,1.,SUM2,PRSUM2)  HG 3100
      WLOSS=VP/VA/F2  HG 3110
      RA1M(J)=SUM1/(SUM2+WLOSS)  HG 3120
      WRITE (6,155) TK(J),RA1M(J)  HG 3130
      WRITE (6,161)  HG 3140
      WRITE (6,163) SUM1,PRSUM1  HG 3150
      SEV=SEV+SUM1*PRSUM1  HG 3160
      WRITE (6,162)  HG 3170
      WRITE (6,166) WLOSS,SUM2,PRSUM2  HG 3180
      TT=WLOSS+SUM2  HG 3190
      AA=WLOSS/TT  HG 3200
      AR=SUM2/TT  HG 3210
      WRITE (6,148) AA,AH  HG 3220
123    CONTINUE  HG 3230
      XL(2,J,J,11)=(RNIO+RA1M(1)+RA1M(2))*VP*XNO*100.  HG 3240
      XNM=-RA1M(1)+RA1M(2)  HG 3250
      IF (11,GT,1) XNM=2.*XNM-SD(5,J,J,11)/100.  HG 3260
C      CALCULATION OF DOUBLE/NEUTRAL RATIO  HG 3270
C      HG 3280
C      CALL YINTEG (SAO2,SEO2,1.,SUM1,PRSUM1)  HG 3290

```

```

CALL YINTEG (S212,SE12,PR10,SUM2,PRSUM2)
CALL SUMIT (S212,SE12,2,RA1M0,TSUM1,B,C)
WLOSS=1.4142*VP/VA/F2
RK=0.
SD(5,JJ,II)=(RA1M0(1)+RA1M0(2))*100.
DO 124 I=1,2
124  RW=RW+RA0M0(I)*SUMM
    RI=0.
    DO 125 I=1,NG
125  RL=RL+RR(I)*SUMM
    R20=(SUM1+SUM2+TSUM1+RK+RL)/WLOSS
C
C PREDICTION OF NEXT DOUBLE ION/NEUTRAL FOR USE IN PREDICTION
C OF NEUTRAL DENSITY
C
    IF (II.EQ.1) GO TO 126
    II=II-1
    XN2=(2.*R20-SD(5,JJ,II)*.01)*2.
    GO TO 127
126  XN2=2.*R20
127  CONTINUE
    SD(1,JJ,II)=R20*XN0
    SD(2,JJ,II)=R20*XA
    XL(3,JJ,II)=R20*VP*1.4142*XN0*100.
    SD(6,JJ,II)=R20*100.
C
C WRITE DOUBLE/NEUTRAL RATIO, ETC.
C
    WRITE (6,156) R20
    G(II)=PRIMRG
    PN=PR(R,C)
    WRITE (6,161)
    WRITE (6,165) SUM1,PRSUM1,SUM2,PRSUM2,TSUM1,PN,RK,PRSUMM
    SAV=SAV+SUM1*PRSUM1+SUM2*PRSUM2+TSUM1*PN+(RK+RL)*PRSUMM
    IT=SUM1+SUM2+TSUM1+RK+RL
    AA=SUM1/IT
    AB=SUM2/IT
    AC=TSUM1/IT
    AD=RK/IT
    AE=RL/IT
    WRITE (6,167) AA,AB,AC,AD
    WRITE (6,163) RL,PRSUMM
    WRITE (6,169) AE
    WRITE (6,162)
    WRITE (6,166) WLOSS
C
C BEAM CURRENT
C
    XXXX=(XL(2,JJ,II)+XL(3,JJ,II)*2.)*1.6E-16*QPC
C
C MASS LOSS RATE
C
    TOTLOSS=(XL(1,JJ,II)*QPC+(XL(2,JJ,II)+XL(3,JJ,II)*2*QPC)*100.
    *AE-16
    GT=XXXXX/TOTLOSS
    SD(9,JJ,II)=GT
C
C EVZION
C
    EVZION=PRIMRG*VZ/(XXXXX*1.6E-16)*QPC*VCL
C
C AEC CURRENT
C
    AEC=1.6E-16*VZ/(XXXXX*1.6E-16)*QPC*VCL
    SD(10,JJ,II)=AEC
    SD(11,JJ,II)=V

```

```

C      WRITE (6,159) XXXX,UTL,EV,ARCI
C      CHECK FOR PLASMA NEUTRALITY
C      EP=ABS((XNM*AN2*RNIO)/XNI-1.)
C      IF (IFLAG.EQ.1.AND.EP.GT..03) GO TO 108
C      PRINRG=PRJNRG*DP
C      IF (IFLAG.NE.0) GO TO 138
128      CONTINUE
129      CONTINUE
C      INTERPOLATION FOR THE ELECTRON DENSITY WHICH YIELDS DESIRED MASS
C      LOSS RATE
C      DO 132 IY=1,NS
C      LOSS RATE
C      DO 131 JZ=1,ND
C      DO 130 JY=1,NS
C      PYP(JY)=(XL(1,JY,JZ)*OPN+(XL(2,JY,JZ)+XL(3,JY,JZ))*OPCHG
C      )*1.6E-16
130      CONTINUE
C      WRITE (6,160) (PYP(JK),JK=1,NS)
C      DO 131 JA=1,NC
C      CALL AITKEN (PYP,XNE,NS,2,PNO(JA),PNE(JA,JZ))
C      IF (PNE(JA,JZ).LT.0.) PNE(JA,JZ)=0.
131      CONTINUE
C      CALCULATE N+/N+
C      DO 132 IZ=1,ND
C      DPP(IY,IZ)=SD(6,IY,IZ)/SD(4,IY,IZ)
132      CONTINUE
C      CALL CRSPLT (PNO,DPP,XNE,PNE,G,X,Y,Z,ND,NS,NC)
C      INTERPOLATION OF PLASMA PROPERTIES ETC. FOR CONSTANT MASS LOSS RATE
C      DO 135 IK=1,13
C      DO 133 IF=1,8
133      Y(IF)=TTI(IK,IF)
C      DO 134 IE=1,NS
C      DO 134 IF=1,ND
134      DPP(IF,IE)=SD(IK,IE,IF)
C      CALL CRSPLT (PNO,DPP,XNE,PNE,G,X,Y,Z,ND,NS,NC)
135      CONTINUE
C      DO 137 L=1,NC
C      DO 136 K=1,25
C      PXP(K)=UTI(L,K)/PNO(L)
136      PYP(K)=PD(L,K)
C      CALL MAP4 (5,PXP,PYP,1,25,HL,HH,VL,VH,QR,QT,Z,1)
137      CALL MAP4 (5,PXP,PYP,1,25,HL,HH,VL,VH,QR,QT,Z,1)
138      CONTINUE
C      139 FORMAT (2X,16HITERATION FOR N+)
C      140 FORMAT (5F10.4)
C      141 FORMAT (5F10.4)
C      142 FORMAT (16I5)
C      143 FORMAT (4F10.4,4F10.2)
C      144 FORMAT (4HV/AF,FA,3,4X,3HEF=,FB,3,3HE1P,4X,2HE=,FC,1,4X,4HP/AF=,FS,4
C      12)
C      145 FORMAT (/3X,14HVOL ZAREA(M+1)=,1,4,5X,14HELEC DEN(M-3)=,F11,4,5H
C      1X,14HELEC TEMP(EV)=,F7,3,5X,16H P-1, ENERGY(EV)=,F7,3,5X,6HNP/NN=,F8
C      26,5)
C      146 FORMAT (/10X,10HVOL (C43)=,F10,3,10X,7HA-NEUT=,F10,3,10X,10MA-+
C      1CM2)=,F10,3,3X, 3HE1=,F6,2,3X, 3HE2=,F6,2)

```

```

147 FORMAT (///,20X,A10,5X,5HNMETA/NO=,F10.5) HG 4620
148 FORMAT (10X,F10.5,21X,2(F10.5,20X)) HG 4630
149 FORMAT (///,10X,23HNEUTRAL DENSITY (CM-3)=,F10.3,10X,15HNO. ITERATING HG 4640
10NS=,14) HG 4650
150 FORMAT (///,20X,A10,5X,8HNEFS/NO=,F10.6,10X,20HMEAN FREE PATH (CM)=HG 4660
1.FR,5) HG 4670
151 FORMAT (11X,F10.5,20X,3(F10.5,20X)) HG 4680
152 FORMAT (10X,F11.4,20X,F11.4,20X,2(F11.4,1X,E9.2,10X)) HG 4690
153 FORMAT (///,20X,6HN+/NO=,F10.5) HG 4700
154 FORMAT (10X,3(F10.5,20X)) HG 4710
155 FORMAT (///,20X,A10,5X,10HN+META/NO=,F10.5) HG 4720
156 FORMAT (///,20X,7HN+/NO=,F10.5) HG 4730
157 FORMAT (10X,4(F10.5,21X),/) HG 4740
158 FORMAT (10X,F10.5) HG 4750
159 FORMAT (/,5X,5HHEAM=,F10.3,3HMA.,10X,12HUTILIZATION=,F10.6,10X,16HHG 4760
1EV PER REAM 10N=,F10.5,10X,5H1ARC=,F10.3) HG 4770
160 FORMAT (/,2X,3HM/A,8(3X,F10.1)) HG 4780
161 FORMAT (/,20X,49HNUMERATOR TERMS (1/SEC) FOLLOWED BY PRI. FRACTIONHG 4790
1) HG 4800
162 FORMAT (/,20X,52HDENOMINATOR TERMS FOLLOWED BY PRI. FRACTION (IF AHG 4810
1NY)) HG 4820
163 FORMAT (10X,F11.4,1X,E9.2) HG 4830
164 FORMAT (10X,3(F11.4,1X,E9.2,10X)) HG 4840
165 FORMAT (10X,4(F11.4,1X,E9.2,10X)) HG 4850
166 FORMAT (10X,F11.4,20X,F11.4,1X,E9.2,10X) HG 4860
167 FORMAT (10X,F11.4,20X,2(F11.4,1X,E9.2,10X)) HG 4870
168 FORMAT (3(F10.4,F10.3),20X) HG 4880
C HG 4890
END HG 4900

SUBROUTINE CRSPLT (PNO,UPP,XNE,PNE,G,X,H,Z,ND,NS,NC) CRS 10
C CRS 20
C THIS SUBROUTINE INTERPOLATES IN THE ARRAY DPP TO GET THE VALUES FOR CRS 30
C CONSTANT MASS FLOW RATE (DET. BY PNE) AND THEN PLOTS THE RESULTS CRS 40
C CRS 50
C COMMON /R/ UTL(4,25),PD(4,25),IK CRS 60
C DIMENSION DPP(6,6), PNO(4), XNF(6), PNF(6,10), G(8), PYP(30), PXP(CRS 70
130), PP(30), SP(10,30), X(8), Y(8), H(8), Z(4) CRS 80
C CRS 90
C INTERPOLATION CRS 100
C CRS 110
C DO 102 KZ=1,ND CRS 120
DO 101 KY=1,NS CRS 130
101 PYP(KY)=DPP(KY,KZ) CRS 140
DO 102 KX=1,NC CRS 150
CALL ATIKEN (XNF,PYP,NS,2,PNE(KX,KZ),SP(KX,KZ)) CRS 160
IF (PNE(KX,KZ).GT.1.E14) SP(KX,KZ)=0. CRS 170
IF (PNE(KX,KZ).EQ.0.) SP(KX,KZ)=0. CRS 180
102 CONTINUE CRS 190
C CRS 200
C FIND MAX AND MIN CRS 210
C CRS 220
C DO 104 JO=1,NC CRS 230
DO 103 JP=1,ND CRS 240
103 PP(JP)=SP(JO,JP) CRS 250
104 CALL MAPA (P,G,PP,1,ND,H,HH,VL,VH,X,Y,TI,1) CRS 260
C CRS 270
C PLOT OF DATA CRS 280
C CRS 290
C CALL MAPA (1,PXP,PYP,1,25,HL,HH,VL,VH,X,Y,TI,1) CRS 300
CALL MAPM (1,PXP,PYP,1,25,HL,HH,VL,VH,X,Y,TI,1) CRS 310
DO 112 IA=1,NC CRS 320
DO 105 IH=1,ND CRS 330
105 PP(IH)=SP(IA,IH) CRS 340
CALL XINTERP (G,PP,PXP,PYP,ND,25,3) CRS 350
XX=PNO(IA) CRS 360

```

	WRITE (6,113) XX	CRS 370
	WRITE (6,114) X(1),M(1)	CRS 380
	DO 106 IX=1,25	CRS 390
106	WRITE (6,115) PXP(IX),PYP(IX)	CRS 400
	WRITE (6,116) (PNE(IX,II),II=1,ND)	CRS 410
	WRITE (6,117) (G(IX),FP(IX),IX=1,ND)	CRS 420
C		CRS 430
C	PLOT OF UTILIZATION VERSUS DISCHARGE POWER	CRS 440
C		CRS 450
	IF (IK.EQ.9.OR.IK.EQ.13) GO TO 107	CRS 460
	GO TO 111	CRS 470
107	IF (IK.EQ.13) GO TO 109	CRS 480
	DO 108 L=1,25	CRS 490
108	UTL(IA,L)=PYP(L)	CRS 500
	GO TO 111	CRS 510
109	DO 110 L=1,25	CRS 520
110	PD(IA,L)=PYP(L)	CRS 530
111	CONTINUE	CRS 540
	CALL MAPM (2,PXP,PYP,1,25,HL,HH,VL,VH,X,H,Z,1)	CRS 550
112	CALL MAPA (2,PXP,PYP,1,25,HL,HH,VL,VH,X,H,Z,1)	CRS 560
	CALL MAPA (4,PXP,PYP,1,25,HL,HH,VL,VH,X,H,Z,1)	CRS 570
	CALL MAPM (4,PXP,PYP,1,25,HL,HH,VL,VH,X,H,Z,1)	CRS 580
	RETURN	CRS 590
C		CRS 600
113	FORMAT (//,20X,13HPICKED VALUE=,2X,E10.3,9HMILLIAMPS)	CRS 610
114	FORMAT (/,10X,A10,20X,A10)	CRS 620
115	FORMAT (12X,F4.3,18X,F11.4,10X,E11.4)	CRS 630
116	FORMAT (/,5X,10HFLEC.DFENS,.8(2X,F10.3))	CRS 640
117	FORMAT (8F10.3)	CRS 650
C		CRS 660
	END	CRS 670
	SUBROUTINE XINTERP (X,Y,XI,YI,NIN,NOUT,INTERP)	INT 10
C		INT 20
C	THIS SUBROUTINE RETURNS -NOUT- POINTS WHICH ARE INTERPOLATED TO	INT 30
C	THE -INTERP- DEGREE FROM -X,Y-	INT 40
C		INT 50
	DIMENSION X(NIN), Y(NIN), XI(NOUT), YI(NOUT)	INT 60
	DX=(X(NIN)-X(1))/FLOAT(NOUT-1)	INT 70
	XX=X(1)	INT 80
	DO 101 I=1,NOUT	INT 90
	XI(I)=XX	INT 100
	CALL AITKEN (X,Y,NIN,INTERP,XX,YY)	INT 110
	IF (YY.LT.0.) YY=0.	INT 120
	YI(I)=YY	INT 130
101	XX=XX+DX	INT 140
	RETURN	INT 150
C		INT 160
	END	INT 170
	SUBROUTINE YINTEG (SIGMA,SIGNRG,PROP,SUM,PRSUM)	NTG 10
C		NTG 20
C	EVALUATION OF REACTION RATE	NTG 30
C		NTG 40
	COMMON /A/ NP,NM,T,PRINRG	NTG 50
	DIMENSION SIGMA(2,21), SIGNRG(2,21), S(21), SE(21)	NTG 60
	REAL NP,NM	NTG 70
C		NTG 80
C	PRIMARY ELECTRONS	NTG 90
C		NTG 100
	DO 101 I=1,21	NTG 110
	SX(I)=SIGMA(1,I)	NTG 120
101	SE(I)=SIGNRG(1,I)	NTG 130
	CALL AITKEN (SE,SX,21,2,PRINRG,XX)	NTG 140
	PRSUM=NP*PRINRG*XX	NTG 150
C		NTG 160



C	MAXWELLIAN ELECTRONS	NTG	170
C		NTG	180
	DO 102 I=1,21	NTG	190
	SX(I)=SIGMA(2,I)	NTG	200
102	SF(I)=SIGNRG(2,I)	NTG	210
	CALL AITKEN (SF,SX,21,2,T,TR)	NTG	220
	TSUM=PROP*NM*TR	NTG	230
	SUM=TSUM+PSUM	NTG	240
	PRSUM=PSUM/SUM	NTG	250
	RETURN	NTG	260
C		NTG	270
	END	NTG	280
	SUBROUTINE SUMIT (SIG,SGF,N,PROP,TSUM,SUMS,PRSUMS)	SUM	10
C		SUM	20
C	TRANSFER ROUTINE FOR EXCITED STATES	SUM	30
C		SUM	40
	COMMON /A/ NP,NM,TEMP,PRINRG	SUM	50
	DIMENSION SIG(N,2,21), SGE(N,2,21), PROP(N), SUMS(N), PRSUMS(N),	SSUM	60
	IX(2,25), SF(2,25)	SUM	70
	REAL NP,NM	SUM	80
C		SUM	90
C	CALCULATES THE SUM OF INTERGALS	SUM	100
C		SUM	110
	TSUM=0.	SUM	120
	DO 102 I=1,N	SUM	130
	DO 101 J=1,2	SUM	140
	DO 101 K=1,21	SUM	150
	SX(J,K)=SIG(I,J,K)	SUM	160
101	SF(J,K)=SGF(I,J,K)	SUM	170
	CALL YNTEG (SX,SE,PROP(I),SUMS(I),PRSUMS(I))	SUM	180
102	TSUM=TSUM+SUMS(I)	SUM	190
	RETURN	SUM	200
C		SUM	210
	END	SUM	220
	SUBROUTINE AITKEN (X,Y,N,K,XR,YR)	AIT	10
C		AIT	20
C	*****	AIT	30
C		AIT	40
C	AITKEN INTERPOLATION SUBROUTINE	AIT	50
C	CALLING SEQUENCE...	AIT	60
C	CALL AITKEN(X,Y,N,K,XR,YR)	AIT	70
C	X IS A ONE DIMENSIONAL ARRAY OF INDEPENDENT	AIT	80
C	VARIABLE(INCREASING OR DECREASING)	AIT	90
C	Y IS A ONE DIMENSIONAL ARRAY OF DEPENDENT	AIT	100
C	VARIABLE	AIT	110
C	N IS NO. OF X,Y PAIRS	AIT	120
C	K IS DEGREE OF INTERPOLATING POLYNOMIAL (MAX = 10 )	AIT	130
C	XR IS INDEP. VARIABLE ARGUMENT	AIT	140
C	YR IS INTERPOLATED RESULT	AIT	150
C		AIT	160
C	*****	AIT	170
C		AIT	180
C	TYPE, DIMENSION AND LABELED COMMON STATEMENTS	AIT	190
C		AIT	200
	DIMENSION X(N), Y(N), XX(11), YY(11)	AIT	210
	K1=K+1	AIT	220
	IF (X(N)-X(1)) 110,101,101	AIT	230
101	IF (XR-X(1)) 102,102,103	AIT	240
102	LL=0	AIT	250
	GO TO 119	AIT	260
C		AIT	270
	103 IF (X(N)-XR) 104,104,105	AIT	280
	104 LL=K-K1	AIT	290
	GO TO 119	AIT	300

C	105 LL=1	AIT 310			
	LU=N	AIT 320			
	106 IF (LU-LL-1) 117,117,107	AIT 330			
	107 LI=(LL+LU)/2	AIT 340			
	IF (X(LI)-XR) 109,108,109	AIT 350			
	108 LL=LI	AIT 360			
	GO TO 106	AIT 370			
C	109 LU=LI	AIT 380			
	GO TO 106	AIT 390			
C	110 IF (XB-X(1)) 111,102,102	AIT 400			
	111 IF (X(N)-XR) 112,104,104	AIT 410			
	112 LL=1	AIT 420			
	LU=N	AIT 430			
	113 IF (LU-LL-1) 117,117,114	AIT 440			
	114 LI=(LL+LU)/2	AIT 450			
	IF (X(LI)-XB) 115,116,116	AIT 460			
	115 LU=LI	AIT 470			
	GO TO 113	AIT 480			
C	116 LL=LI	AIT 490			
	GO TO 113	AIT 500			
C	117 LL=LL-(K1+1)/2	AIT 510			
	IF (LL) 102,119,118	AIT 520			
	118 IF (LL+K1-N) 119,119,104	AIT 530			
	119 DO 120 I=1,K1	AIT 540			
	II=LL+I	AIT 550			
	XX(I)=X(II)-XR	AIT 560			
	120 YY(I)=Y(II)	AIT 570			
	DO 121 I=1,K	AIT 580			
	DO 121 J=1,K	AIT 590			
	IF (XX(J+1).EQ.XX(I)) GO TO 122	AIT 600			
	121 YY(J+1)=(1./(XX(J+1)-XX(I)))*(YY(I)*XX(J+1)-YY(J+1)*XX(I))	AIT 610			
	YR=YY(K1)	AIT 620			
	RETURN	AIT 630			
	122 WRITE (6,123) (X(I),I=1,N)	AIT 640			
	WRITE (6,123) (Y(I),I=1,N)	AIT 650			
	WRITE (6,124)	AIT 660			
	A=1./(XX(J+1)-XX(I))	AIT 670			
	CCC=3.*A	AIT 680			
	RETURN	AIT 690			
C	123 FORMAT (10(2X,F10.3))	AIT 700			
	124 FORMAT (10X,17#TROUBLE IN AITKEN)	AIT 710			
C	END	AIT 720			
		AIT 730			
		AIT 740			
		AIT 750			
		AIT 760			
		AIT 770			
		AIT 780			
		AIT 790			
R	5.0000 0.	6.0000 0.	7.0000 0.	HG-HG+	1
	8.0000 0.	9.0000 0.	10.0000 0.	HG-HG+	2
	11.0000 .624E-14	12.0000 .164E-13	14.0000 .339E-13HG-HG+		3
	16.0000 .506E-13	18.0000 .573E-13	20.0000 .837E-13HG-HG+		4
	23.5000 .111E-12	27.0000 .136E-12	30.0000 .153E-12HG-HG+		5
	33.5000 .172E-12	37.0000 .184E-12	40.0000 .198E-12HG-HG+		6
	42.0000 .205E-12	44.0000 .211E-12	50.0000 .230E-12HG-HG+		7
	3.0000 .225E-14	4.0000 .533E-14	4.3000 .742E-14HG-HG+		1
	4.7000 .103E-13	5.0000 .121E-13	5.3000 .141E-13HG-HG+		2
	5.7000 .164E-13	6.0000 .171E-13	6.3000 .214E-13HG-HG+		3
	6.7000 .244E-13	7.0000 .258E-13	7.5000 .308E-13HG-HG+		4
	8.0000 .348E-13	8.5000 .388E-13	9.0000 .429E-13HG-HG+		5
	9.5000 .463E-13	10.0000 .502E-13	10.5000 .549E-13HG-HG+		6
	11.0000 .589E-13	12.0000 .656E-13	13.0000 .740E-13HG-HG+		7
	5.0000 0.	6.0000 0.	7.0000 0.	HG-HG+	1
	8.0000 0.	9.0000 0.	10.0000 0.	HG-HG+	2

11.0000	0.	12.0000	0.	14.0000	0.	HG-HG++	3
16.0000	0.	18.0000	0.	20.0000	0.	HG-HG++	4
23.5000	0.	27.0000	0.	30.0000	0.	.617E-15HG-HG++	5
33.5000	.190E-14	37.0000	.306E-14	40.0000	.434E-14HG-HG++		6
42.0000	.536E-14	44.0000	.648E-14	50.0000	.103F-13HG-HG++		7
3.0000	.322E-18	4.0000	.424E-17	4.3000	.743F-17HG-HG++		1
4.7000	.139E-16	5.0000	.210E-16	5.3000	.304F-16HG-HG++		2
5.7000	.470E-16	6.0000	.629E-16	6.3000	.922F-16HG-HG++		3
6.7000	.114E-15	7.0000	.142E-15	7.5000	.197F-15HG-HG++		4
8.0000	.265F-15	8.5000	.346E-15	9.0000	.434F-15HG-HG++		5
9.5000	.546F-15	10.0000	.665E-15	10.5000	.797F-15HG-HG++		6
11.0000	.942E-15	12.0000	.127E-14	13.0000	.164F-14HG-HG++		7
5.	-3. E-30	7.	-2.5 E-30	8.5	-2. F-30HG+ - HG++		1
10.	-1.5 E-30	12.	-1.25E-30	14.	-1. F-30HG+ - HG++		2
16.	-.5 E-30	18.6	0. E-30	19.25	.162 F-13HG+ - HG++		3
20.	.443 E-13	20.5	.47 E-13	22.	.529 F-13HG+ - HG++		4
25.	.657 E-13	27.5	.766 E-13	30.	.854 F-13HG+ - HG++		5
33.	.941 E-13	37.	1.02 E-13	40.	1.1 E-13HG+ - HG++		6
42.	1.15 E-13	46.	1.24 E-13	50.	1.33 F-13HG+ - HG++		7
3.0000	.267F-15	4.0000	.127E-14	4.3000	.177F-14HG+ - HG++		1
4.7000	.257E-14	5.0000	.327E-14	5.3000	.405E-14HG+ - HG++		2
5.7000	.521E-14	6.0000	.616E-14	6.3000	.717F-14HG+ - HG++		3
6.7000	.860E-14	7.0000	.973E-14	7.5000	.117E-13HG+ - HG++		4
8.0000	.138E-13	8.5000	.159E-13	9.0000	.181F-13HG+ - HG++		5
9.5000	.203F-13	10.0000	.226E-13	10.5000	.249F-13HG+ - HG++		6
11.0000	.272E-13	12.0000	.318F-13	13.0000	.364F-13HG+ - HG++		7
5.0000	.988F-14	6.0000	.121E-13	7.0000	.107F-13HG-HGM 3P0		1
8.0000	.907F-14	9.0000	.744F-14	10.0000	.576F-14HG-HGM 3P0		2
11.0000	.441E-14	12.0000	.333E-14	14.0000	.228F-14HG-HGM 3P0		3
16.0000	.191E-14	18.0000	.123E-14	20.0000	.103F-14HG-HGM 3P0		4
23.5000	.827F-15	27.0000	.720F-15	30.0000	.579F-15HG-HGM 3P0		5
33.5000	.423E-15	37.0000	.286E-15	40.0000	.188F-15HG-HGM 3P0		6
42.0000	0.	44.0000	0.	50.0000	0.	HG-HGM 3P0	7
3.0000	.318F-14	4.0000	.378E-14	4.3000	.367F-14HG-HGM 3P0		1
4.7000	.395E-14	5.0000	.348F-14	5.3000	.394F-14HG-HGM 3P0		2
5.7000	.393F-14	6.0000	.346F-14	6.3000	.393F-14HG-HGM 3P0		3
6.7000	.388F-14	7.0000	.384F-14	7.5000	.376E-14HG-HGM 3P0		4
8.0000	.367F-14	8.5000	.358F-14	9.0000	.348F-14HG-HGM 3P0		5
9.5000	.339F-14	10.0000	.340E-14	10.5000	.321F-14HG-HGM 3P0		6
11.0000	.312E-14	12.0000	.244E-14	13.0000	.278F-14HG-HGM 3P0		7
5.0000	0.	6.0000	.437E-13	7.0000	.482E-13HG-HGM 3P2		1
8.0000	.404F-13	9.0000	.324F-13	10.0000	.260F-13HG-HGM 3P2		2
11.0000	.212F-13	12.0000	.185E-13	14.0000	.136F-13HG-HGM 3P2		3
16.0000	.105F-13	18.0000	.799F-14	20.0000	.655F-14HG-HGM 3P2		4
23.5000	.433F-14	27.0000	.312E-14	30.0000	.227F-14HG-HGM 3P2		5
33.5000	.168F-14	37.0000	.144E-14	40.0000	.131F-14HG-HGM 3P2		6
42.0000	.113F-14	44.0000	.916E-15	50.0000	.365F-15HG-HGM 3P2		7
3.0000	.963F-14	4.0000	.125F-13	4.3000	.130F-13HG-HGM 3P2		1
4.7000	.135F-13	5.0000	.138F-13	5.3000	.140F-13HG-HGM 3P2		2
5.7000	.142E-13	6.0000	.143E-13	6.3000	.143E-13HG-HGM 3P2		3
6.7000	.147F-13	7.0000	.142E-13	7.5000	.141F-13HG-HGM 3P2		4
8.0000	.139F-13	8.5000	.137F-13	9.0000	.134F-13HG-HGM 3P2		5
9.5000	.132F-13	10.0000	.124F-13	10.5000	.126E-13HG-HGM 3P2		6
11.0000	.123F-13	12.0000	.118E-13	13.0000	.112F-13HG-HGM 3P2		7
5.0000	.448F-14	6.0000	.961E-14	7.0000	.462F-14HG-HGM 3P1		1
8.0000	.410E-14	9.0000	.624F-14	10.0000	.714F-14HG-HGM 3P1		2
11.0000	.708F-14	12.0000	.606E-14	14.0000	.628F-14HG-HGM 3P1		3
16.0000	.640E-14	18.0000	.641E-14	20.0000	.633F-14HG-HGM 3P1		4
23.5000	.695E-14	27.0000	.527E-14	30.0000	.444F-14HG-HGM 3P1		5
33.5000	.319F-14	37.0000	.161F-14	40.0000	0.	HG-HGM 3P1	6
42.0000	0.	44.0000	0.	50.0000	0.	HG-HGM 3P1	7
3.0000	.234F-14	4.0000	.315E-14	4.3000	.334F-14HG-HGM 3P1		1
4.7000	.356F-14	5.0000	.371E-14	5.3000	.384F-14HG-HGM 3P1		2
5.7000	.308F-14	6.0000	.408F-14	6.3000	.416F-14HG-HGM 3P1		3
6.7000	.426F-14	7.0000	.432E-14	7.5000	.434F-14HG-HGM 3P1		4
8.0000	.445F-14	8.5000	.449F-14	9.0000	.451F-14HG-HGM 3P1		5

9.5000	.452F-14	10.0000	.451E-14	10.5000	.450F-14HG-HGR	3P1	6
11.0000	.448F-14	12.0000	.441E-14	13.0000	.433F-14HG-HGR	3P1	7
5.0000	0.	6.0000	0.	7.0000	.132F-13HG-HGR	1P1	1
8.0000	.349F-13	9.0000	.579F-13	10.0000	.818F-13HG-HGR	1P1	2
11.0000	.106E-12	12.0000	.130E-12	14.0000	.162F-12HG-HGR	1P1	3
16.0000	.179F-12	18.0000	.189E-12	20.0000	.194F-12HG-HGR	1P1	4
23.5000	.209F-12	27.0000	.216E-12	30.0000	.220F-12HG-HGR	1P1	5
33.5000	.223F-12	37.0000	.224E-12	40.0000	.224F-12HG-HGR	1P1	6
42.0000	.224F-12	44.0000	.224E-12	50.0000	.222F-12HG-HGR	1P1	7
3.0000	.166F-13	4.0000	.323E-13	4.3000	.372F-13HG-HGR	1P1	1
4.7000	.437E-13	5.0000	.485E-13	5.3000	.532F-13HG-HGR	1P1	2
5.7000	.594E-13	6.0000	.634E-13	6.3000	.682F-13HG-HGR	1P1	3
6.7000	.737F-13	7.0000	.777E-13	7.5000	.841E-13HG-HGR	1P1	4
8.0000	.901E-13	8.5000	.957E-13	9.0000	.101F-12HG-HGR	1P1	5
9.5000	.106F-12	10.0000	.111E-12	10.5000	.115F-12HG-HGR	1P1	6
11.0000	.119F-12	12.0000	.127E-12	13.0000	.133F-12HG-HGR	1P1	7
5.0000	0.	6.0000	.451E-15	7.0000	.865F-14HGM-HG	3P0	1
8.0000	.233F-13	9.0000	.355F-13	10.0000	.477F-13HGM-HG	3P0	2
11.0000	.590F-13	12.0000	.701E-13	14.0000	.916F-13HGM-HG	3P0	3
16.0000	.110F-12	18.0000	.130E-12	20.0000	.157E-12HGM-HG	3P0	4
23.5000	.209F-12	27.0000	.247E-12	30.0000	.278F-12HGM-HG	3P0	5
33.5000	.309F-12	37.0000	.335E-12	40.0000	.354F-12HGM-HG	3P0	6
42.0000	.365F-12	44.0000	.376E-12	50.0000	.400F-12HGM-HG	3P0	7
3.0000	.103E-13	4.0000	.210E-13	4.3000	.247F-13HGM-HG	3P0	1
4.7000	.294E-13	5.0000	.338E-13	5.3000	.378F-13HGM-HG	3P0	2
5.7000	.433F-13	6.0000	.476E-13	6.3000	.518E-13HGM-HG	3P0	3
6.7000	.575F-13	7.0000	.614E-13	7.5000	.690F-13HGM-HG	3P0	4
8.0000	.762F-13	8.5000	.834E-13	9.0000	.904F-13HGM-HG	3P0	5
9.5000	.974E-13	10.0000	.104E-12	10.5000	.111F-12HGM-HG	3P0	6
11.0000	.118F-12	12.0000	.131E-12	13.0000	.143F-12HGM-HG	3P0	7
5.0000	.682F-15	6.0000	.954F-14	7.0000	.312F-13HGM-HG	3P2	1
8.0000	.484F-13	9.0000	.652F-13	10.0000	.798F-13HGM-HG	3P2	2
11.0000	.929F-13	12.0000	.106E-12	14.0000	.129F-12HGM-HG	3P2	3
16.0000	.149F-12	18.0000	.169E-12	20.0000	.147E-12HGM-HG	3P2	4
23.5000	.244F-12	27.0000	.245E-12	30.0000	.316F-12HGM-HG	3P2	5
33.5000	.346F-12	37.0000	.371E-12	40.0000	.390F-12HGM-HG	3P2	6
42.0000	.400F-12	44.0000	.410E-12	50.0000	.433F-12HGM-HG	3P2	7
3.0000	.176F-13	4.0000	.327E-13	4.3000	.375F-13HGM-HG	3P2	1
4.7000	.442F-13	5.0000	.492F-13	5.3000	.542E-13HGM-HG	3P2	2
5.7000	.610E-13	6.0000	.661E-13	6.3000	.711F-13HGM-HG	3P2	3
6.7000	.773F-13	7.0000	.828F-13	7.5000	.911F-13HGM-HG	3P2	4
8.0000	.992F-13	8.5000	.107E-12	9.0000	.115F-12HGM-HG	3P2	5
9.5000	.123F-12	10.0000	.130E-12	10.5000	.138F-12HGM-HG	3P2	6
11.0000	.145F-12	12.0000	.159E-12	13.0000	.172F-12HGM-HG	3P2	7
5.0000	0.	6.0000	0.	7.0000	0.	HGM+ HG+5	1
8.0000	0.	9.0000	0.	10.0000	0.	HGM+ HG+5	2
11.0000	0.	12.0000	0.	14.0000	0.	HGM+ HG+5	3
16.0000	0.	18.0000	0.	20.0000	.625F-15HGM+ HG+5		4
23.5000	.722F-14	27.0000	.238E-13	30.0000	.396F-13HGM+ HG+5		5
33.5000	.576E-13	37.0000	.744E-13	40.0000	.877F-13HGM+ HG+5		6
42.0000	.959F-13	44.0000	.104E-12	50.0000	.124F-12HGM+ HG+5		7
3.0000	.370F-15	4.0000	.261E-15	4.3000	.347F-15HGM+ HG+5		1
4.7000	.842F-15	5.0000	.379E-15	5.3000	.116F-14HGM+ HG+5		2
5.7000	.162E-14	6.0000	.202E-14	6.3000	.247F-14HGM+ HG+5		3
6.7000	.315F-14	7.0000	.372E-14	7.5000	.477F-14HGM+ HG+5		4
8.0000	.544E-14	8.5000	.722E-14	9.0000	.410F-14HGM+ HG+5		5
9.5000	.101E-13	10.0000	.118E-13	10.5000	.134F-13HGM+ HG+5		6
11.0000	.149F-13	12.0000	.185E-13	13.0000	.221F-13HGM+ HG+5		7
5.0000	0.	6.0000	0.	7.0000	0.	HGM+ HG+3	1
8.0000	0.	9.0000	0.	10.0000	0.	HGM+ HG+3	2
11.0000	0.	12.0000	0.	14.0000	0.	HGM+ HG+3	3
16.0000	0.	18.0000	0.	20.0000	.625F-15HGM+ HG+3		4
23.5000	.722F-14	27.0000	.238E-13	30.0000	.396F-13HGM+ HG+3		5
33.5000	.576E-13	37.0000	.744E-13	40.0000	.877F-13HGM+ HG+3		6
42.0000	.959F-13	44.0000	.104E-12	50.0000	.124F-12HGM+ HG+3		7
3.0000	.370F-15	4.0000	.261E-15	4.3000	.347F-15HGM+ HG+3		1
4.7000	.842F-15	5.0000	.379E-15	5.3000	.116F-14HGM+ HG+3		2
5.7000	.162E-14	6.0000	.202E-14	6.3000	.247F-14HGM+ HG+3		3
6.7000	.315F-14	7.0000	.372E-14	7.5000	.477F-14HGM+ HG+3		4
8.0000	.544E-14	8.5000	.722E-14	9.0000	.410F-14HGM+ HG+3		5
9.5000	.101E-13	10.0000	.118E-13	10.5000	.134F-13HGM+ HG+3		6
11.0000	.149F-13	12.0000	.185E-13	13.0000	.221F-13HGM+ HG+3		7
5.0000	0.	6.0000	0.	7.0000	0.	HGM+ HG+1	1
8.0000	0.	9.0000	0.	10.0000	0.	HGM+ HG+1	2
11.0000	0.	12.0000	0.	14.0000	0.	HGM+ HG+1	3
16.0000	0.	18.0000	0.	20.0000	.625F-15HGM+ HG+1		4
23.5000	.722F-14	27.0000	.238E-13	30.0000	.396F-13HGM+ HG+1		5
33.5000	.576E-13	37.0000	.744E-13	40.0000	.877F-13HGM+ HG+1		6
42.0000	.959F-13	44.0000	.104E-12	50.0000	.124F-12HGM+ HG+1		7
3.0000	.370F-15	4.0000	.261E-15	4.3000	.347F-15HGM+ HG+1		1

4.7000	.642F-15	5.0000	.872F-15	5.3000	.116E-14HGM+-HG++3	2
5.7000	.162F-14	6.0000	.202F-14	6.3000	.247F-14HGM+-HG++3	3
6.7000	.315F-14	7.0000	.372F-14	7.5000	.477F-14HGM+-HG++3	4
8.0000	.594F-14	8.5000	.722F-14	9.0000	.860F-14HGM+-HG++3	5
9.5000	.101F-13	10.0000	.116F-13	10.5000	.133F-13HGM+-HG++3	6
11.0000	.149F-13	12.0000	.185F-13	13.0000	.221F-13HGM+-HG++3	7
5.0000	0.	6.0000	.221F-14	7.0000	.129F-13HGR-HG+3P1	1
8.0000	.289F-13	9.0000	.423F-13	10.0000	.553F-13HGR-HG+3P1	2
11.0000	.670F-13	12.0000	.787F-13	14.0000	.101F-12HGR-HG+3P1	3
16.0000	.119F-12	18.0000	.140F-12	20.0000	.167F-12HGR-HG+3P1	4
23.5000	.214F-12	27.0000	.256F-12	30.0000	.288F-12HGR-HG+3P1	5
33.5000	.318F-12	37.0000	.344F-12	40.0000	.363F-12HGR-HG+3P1	6
42.0000	.374F-12	44.0000	.384F-12	50.0000	.409F-12HGR-HG+3P1	7
3.0000	.119F-13	4.0000	.237F-13	4.3000	.276F-13HGR-HG+3P1	1
4.7000	.331F-13	5.0000	.373F-13	5.3000	.416F-13HGR-HG+3P1	2
5.7000	.475F-13	6.0000	.519F-13	6.3000	.553F-13HGR-HG+3P1	3
6.7000	.623F-13	7.0000	.664F-13	7.5000	.743F-13HGR-HG+3P1	4
8.0000	.817F-13	8.5000	.890F-13	9.0000	.963F-13HGR-HG+3P1	5
9.5000	.103F-12	10.0000	.111E-12	10.5000	.117F-12HGR-HG+3P1	6
11.0000	.124F-12	12.0000	.137F-12	14.0000	.150F-12HGR-HG+3P1	7
5.0000	0.	6.0000	0.	7.0000	.793F-15HGR-HG+1P1	1
8.0000	.628F-14	9.0000	.161E-13	10.0000	.246F-13HGR-HG+1P1	2
11.0000	.338F-13	12.0000	.435E-13	14.0000	.525F-13HGR-HG+1P1	3
16.0000	.793F-13	18.0000	.984E-13	20.0000	.126F-12HGR-HG+1P1	4
23.5000	.173F-12	27.0000	.215E-12	30.0000	.247F-12HGR-HG+1P1	5
33.5000	.279F-12	37.0000	.305E-12	40.0000	.325F-12HGR-HG+1P1	6
42.0000	.336F-12	44.0000	.347F-12	50.0000	.372F-12HGR-HG+1P1	7
3.0000	.585F-14	4.0000	.134F-13	4.3000	.162F-13HGR-HG+1P1	1
4.7000	.201F-13	5.0000	.233F-13	5.3000	.265F-13HGR-HG+1P1	2
5.7000	.311F-13	6.0000	.346F-13	6.3000	.382F-13HGR-HG+1P1	3
6.7000	.431F-13	7.0000	.468F-13	7.5000	.511F-13HGR-HG+1P1	4
8.0000	.595F-13	8.5000	.659F-13	9.0000	.722F-13HGR-HG+1P1	5
9.5000	.788F-13	10.0000	.849F-13	10.5000	.912F-13HGR-HG+1P1	6
11.0000	.974F-13	12.0000	.109E-12	13.0000	.121F-12HGR-HG+1P1	7
5.0000	.174E-13	6.0000	.188E-13	7.0000	.200F-13HG+-HGM+	5
8.0000	.210E-13	9.0000	.219E-13	10.0000	.227E-13HG+-HGM+	5
11.0000	.235E-13	12.0000	.241E-13	14.0000	.250E-13HG+-HGM+	5
16.0000	.216E-13	18.0000	.190E-13	20.0000	.164E-13HG+-HGM+	5
23.5000	.137E-13	27.0000	.113E-13	30.0000	.967F-14HG+-HGM+	5
33.5000	.817E-14	37.0000	.647E-14	40.0000	.613F-14HG+-HGM+	5
42.0000	.564E-14	44.0000	.521E-14	50.0000	.415F-14HG+-HGM+	5
3.0000	.806E-14	4.0000	.108E-13	4.3000	.114F-13HG+-HGM+	5
4.7000	.122F-13	5.0000	.126F-13	5.3000	.130F-13HG+-HGM+	5
5.7000	.135F-13	6.0000	.138F-13	6.3000	.140F-13HG+-HGM+	5
6.7000	.143F-13	7.0000	.144F-13	7.5000	.146F-13HG+-HGM+	5
8.0000	.147F-13	8.5000	.148E-13	9.0000	.148F-13HG+-HGM+	5
9.5000	.148F-13	10.0000	.148E-13	10.5000	.147E-13HG+-HGM+	5
11.0000	.146E-13	12.0000	.144E-13	14.0000	.141F-13HG+-HGM+	5
5.0000	0.	6.0000	0.	7.0000	.154F-13HG+-HGM+	3
8.0000	.164E-13	9.0000	.173E-13	10.0000	.151E-13HG+-HGM+	3
11.0000	.188E-13	12.0000	.196E-13	14.0000	.202E-13HG+-HGM+	3
16.0000	.186E-13	18.0000	.157E-13	20.0000	.113E-13HG+-HGM+	3
23.5000	.112E-13	27.0000	.922E-14	30.0000	.789E-14HG+-HGM+	3
33.5000	.664E-14	37.0000	.565E-14	40.0000	.499E-14HG+-HGM+	3
42.0000	.455E-14	44.0000	.421E-14	50.0000	.355E-14HG+-HGM+	3
3.0000	.413E-14	4.0000	.646E-14	4.3000	.600E-14HG+-HGM+	3
4.7000	.754E-14	5.0000	.747E-14	5.3000	.547E-14HG+-HGM+	3
5.7000	.882E-14	6.0000	.911E-14	6.3000	.937E-14HG+-HGM+	3
6.7000	.967E-14	7.0000	.993E-14	7.5000	.101E-13HG+-HGM+	3
8.0000	.103E-13	8.5000	.103E-13	9.0000	.106E-13HG+-HGM+	3
9.5000	.106E-13	10.0000	.107E-13	10.5000	.107E-13HG+-HGM+	3
11.0000	.107E-13	12.0000	.107E-13	14.0000	.107E-13HG+-HGM+	3
1	1	6	1			
1.	1.	4.2	27.5	2.4	9.4	11.5
.014						

## APPENDIX B

The computer program "PROP" is listed below. It can be used to determine the values of the volume averaged plasma properties and the uniformity factors needed by the computer program "HG." The data needed to determine these quantities is obtained from a Langmuir probe survey of the discharge chamber in which the plasma properties are determined at many different locations within the chamber. This data is used to numerically evaluate Equations (10) to (15) and (21) yielding the volume averaged plasma properties and the uniformity factors. Comment cards are included in the computer program to indicate the purpose of each section. A CDC 6400 computer will use approximately thirty seconds of Central Processor time to evaluate five sets of data obtained from five Langmuir probe surveys.

```

C      PROGRAM PROP (INPUT,OUTPUT,TAPE5=INPUT,TAPE6=OUTPUT)
C
C      THIS PROGRAM CALCULATES THE AVERAGE PROPERTIES
C      PLS-RADIAL POSITION OF LANGMUIR PROBE POINTS (1-CENTERLINE)
C      POS-POS. OF DESIRED DATA POINTS IF NR.NE.4
C      POSZ-AXIAL POSITION OF LANGMUIR PROBE POSITIONS (1-UPSTREAM PNT.)
C      NT-NO. OF TRACES PER SET      NH-NO. OF RADIAL POINTS
C      IFLAG=1 IF ONE WANTS TO PRODUCE A SET OF POINTS UPSTREAM
C      IFLAG=2 POINTS PRODUCED AT THE BAFFLE
C      DIS-DISTANCE FROM SCREEN TO POINT WHERE THE GENERATED SET IS TO
C      BE PLACED
C      RCATH-CATHODE RADIUS
C      ENP-LENGTH OF PRIMARY ELECTRON REGION AT CENTERLINE
C
C      DIMENSION XNP(72), YNP(72), T(70), Z(70), V(50), ZI(21), G(21), F(PPR
121), TF(21), AA(5), RH(5), CC(5), DD(5), EE(5), FF(5), FND(11), POPRP
25(5), W(11), POSZ(11), YT(11), YP(11), YM(11), YZ(11), POR(10), AAPRP
3A(10), VF(51)
C      DIMENSION AT(70), AZ(70), ANP(70), ANM(70), A(11), H(11), C(11), DPRP
1(11), E(11), VT(11), PLS(5)
C      DATA AA,RH,CC,DD,EE/25*0./
C      DATA POS /0.,1.1,2.2,3.3,4./
C      DATA PLS /0.,1.,2.,3.,3.5/
C
C      INTEGRATED CROSS SECTIONS FOR * TO *
C
C      READ (5,129) (ZI(I),F(I),I=1,21)
C      READ (5,129) (TF(I),G(I),I=1,21)
C      WRITE (6,133) (ZI(I),F(I),I=1,21)
C      WRITE (6,133) (TF(I),G(I),I=1,21)
C      PI=6.2832
101 READ (5,126) NR,NT,IFLAG,DIS,RCATH,ENP
C      IF (FOF(5)) 125,102,125
102 ND=NT/NH
C      NN=ND
C      IF (IFLAG.NE.0) NN=ND+1
C      READ (5,127) (POSZ(I),I=1,ND)
C
C      RADIAL DISTANCE TO CRITICAL FIELD LINE
C
C      READ (5,127) (FND(I),I=1,NN)
C
C      READ IN THE PROPERTIES
C
C      DO 103 I=1,NT
103 READ (5,130) T(I),Z(I),XNP(I),XNM(I)
C      IF (NR.EQ.4) GO TO 104
C      IS=0
C      DO 106 J=1,VT*NR
C      NND=J*NR-1
C      DO 104 J=1,NND
C      K=J+1-I
C      YT(K)=T(J)
C      YP(K)=XNP(J)
C      YM(K)=XNM(J)
104 YZ(K)=Z(J)
C      DO 105 J=1,4
C      I=J+IS
C      CALL ATIKEN (PLS,YT,NN+1,POSZ(J),AT(I))
C      CALL ATIKEN (PLS,YP,NN+1,POSZ(J),ANP(I))
C      CALL ATIKEN (PLS,YM,NN+1,POSZ(J),ANM(I))
105 CALL ATIKEN (PLS,YZ,NN+1,POSZ(J),AZ(I))
106 IS=IS+4
C      NT=NT%NR
C      ND=NT/4

```

```

PRP 10
PRP 20
PRP 30
PRP 40
PRP 50
PRP 60
PRP 70
PRP 80
PRP 90
PRP 100
PRP 110
PRP 120
PRP 130
PRP 140
PRP 150
PRP 160
PRP 170
PRP 180
PRP 190
PRP 200
PRP 230
PRP 210
PRP 220
PRP 240
PRP 250
PRP 260
PRP 270
PRP 280
PRP 290
PRP 300
PRP 310
PRP 320
PRP 330
PRP 340
PRP 350
PRP 360
PRP 370
PRP 380
PRP 390
PRP 400
PRP 410
PRP 420
PRP 430
PRP 440
PRP 450
PRP 460
PRP 470
PRP 480
PRP 490
PRP 500
PRP 510
PRP 520
PRP 530
PRP 540
PRP 550
PRP 560
PRP 570
PRP 580
PRP 590
PRP 600
PRP 610
PRP 620
PRP 630
PRP 640
PRP 650

```

DC 107 J=1,NT	PRP 660
T(J)=AT(J)	PRP 670
Z(J)=AZ(J)	PRP 680
XNP(J)=ANP(J)	PRP 690
107 XNM(J)=ANM(J)	PRP 700
WRITE (6,130) (T(N),Z(N),XNP(N),XNM(N),N=1,NT)	PRP 710
108 IF (IFLAG.EQ.0) GO TO 114	PRP 720
C	PRP 730
C     CALCULATION OF THE EXTRA SET OF POINTS	PRP 740
C	PRP 750
N=1	PRP 760
DO 110 I=1,4	PRP 770
L=0	PRP 780
DO 109 J=I,NT,4	PRP 790
L=L+1	PRP 800
YT(L)=T(J)	PRP 810
YP(L)=XNP(J)	PRP 820
YM(L)=XNM(J)	PRP 830
109     YZ(L)=Z(J)	PRP 840
K=NT+I	PRP 850
CALL AITKEN (POSZ,YT,ND,N,DIS,AT(K))	PRP 860
K=NT+I	PRP 870
CALL AITKEN (POSZ,YT,ND,N,DIS,AT(K))	PRP 880
CALL AITKEN (POSZ,YZ,ND,N,DIS,AZ(K))	PRP 890
CALL AITKEN (POSZ,YP,ND,N,DIS,ANP(K))	PRP 900
CALL AITKEN (POSZ,YM,ND,N,DIS,ANM(K))	PRP 910
IF (AT(K).LT.0.) AT(K)=0.0	PRP 920
IF (AZ(K).LT.0.) AZ(K)=0.0	PRP 930
IF (ANP(K).LT.0.) ANP(K)=0.0	PRP 940
IF (ANM(K).LT.0.) ANM(K)=0.0	PRP 950
WRITE (6,128) AT(K),AZ(K),ANP(K),ANM(K)	PRP 960
110 CONTINUE	PRP 970
C	PRP 980
C     RESHUFFLING OF POINTS	PRP 990
C	PRP 1000
ND=ND+1	PRP 1010
NN=ND-1	PRP 1020
XK=FND(ND)	PRP 1030
DO 111 J=1,NN	PRP 1040
J=ND+1-I	PRP 1050
FND(J)=FND(J-1)	PRP 1060
111 POSZ(J)=POSZ(J-1)	PRP 1070
END(1)=XK	PRP 1080
PCSZ(1)=DIS	PRP 1090
NT=NT+4	PRP 1100
ND=NT/4	PRP 1110
DO 112 I=5,NT	PRP 1120
K=NT+5-I	PRP 1130
J=K-4	PRP 1140
T(K)=T(J)	PRP 1150
Z(K)=Z(J)	PRP 1160
XNP(K)=XNP(J)	PRP 1170
112 XNM(K)=XNM(J)	PRP 1180
NTM=NT-3	PRP 1190
DO 113 I=NTM,NT	PRP 1200
J=I-NTM+1	PRP 1210
T(J)=AT(I)	PRP 1220
Z(J)=AZ(I)	PRP 1230
XNP(J)=ANP(I)	PRP 1240
113 XNM(J)=ANM(I)	PRP 1250
C	PRP 1260
C     START OF THE CALCULATIONS	PRP 1270
C	PRP 1280
114 DO 113 I=1,50	PRP 1290
I=I+1	PRP 1300
I=I+1	PRP 1310





ccc

```

CALL XINTERP (X,Y,A,P,NIN,NUSED,INI)
CALL GETG (A,B,C,NUSED)
CALL ALIPEN (A,C,NUSED,INT,XP,YP)
RETURN
C
END
C
SUBROUTINE AREA (XNP,XNM,ANLE,DTR,DIY,NLN,R,VE,VEA)
C
C THIS SUBROUTINE CALCULATES THE PLASMA NONUNIFORMITY FACTORS
C PRY-POINTS (Z) DEFINING PRIMARY FIELD LINE (FROM SCREEN GRID)
C PRR-POINTS (Z) DEFINING PRIMARY FIELD LINE (FROM CENTER LINE)
C NPRE-NO. OF PRIMARY FIELD LINE POINTS
C IFLAG=1 IF LOSSES ARE ALLOWED TO THE CATHODE POLE PIECE
C D1= DISTANCE TO BAFFLE FROM SCREEN
C CZU=POINT WHERE PRIMARY FIELD LINE INTERSECTS CATHODE POLE PIECE
C (IF IFLAG=1)
C
C DIMENSION DTR(5), DIY(10), XI1(11), XI2(11), XI3(11), XI4(11), PPRARA
1(10), PRY(10), P(5), Z(5), XNP(51), XNM(51), Q(5), VE(51), V(5), VARA
2FI1(11), VE2(11), VE3(11), VE4(11)
C REAL I1,I2
C NFLAG=0
C MFLAG=0
C READ (5,107) NPRE,IFLAG,D1,CZU
C CZU=01
C READ (5,111) (PPR(I),PRY(I),I=1,NPRE)
C NRE=NLN*4
C
C BEGIN CALCULATIONS
C SHUFFLE NO. DENSITIES INTO CORRECT ARRAYS
C
C DO 101 I=1,NP*4
C   J=I+1
C   K=I+2
C   L=I+3
C   M=I/4+1
C   VE1(M)=VE(I)
C   VE2(M)=VE(J)
C   VE3(M)=VE(K)
C   VE4(M)=VE(L)
C   XI2(M)=XNP(J)+XNM(J)
C   XI3(M)=XNP(K)+XNM(K)
C   XI4(M)=XNP(L)+XNM(L)
101 XI1(M)=XNP(I)+XNM(I)
C
C WRITE OUT THESE ARRAYS
C
C WRITE (6,116) (XI1(I),I=1,NLN)
C WRITE (6,116) (XI2(I),I=1,NLN)
C WRITE (6,116) (XI3(I),I=1,NLN)
C WRITE (6,116) (XI4(I),I=1,NLN)
C AZ=0.
C DY=PRY(NPRE)/200.
C AN=0.
C AN=0.
C AN=0.
C YZ=DY/2.
C
C BEGIN CALCULATION OF THE CATHODE INTEGRAL
C PRIMARY FIELD LINE SECTION
C
C DO 112 I=1,400
C   IF (I/4+1) GO TO 1122.
C   YI=XI1(I)/YZ.
C   YI=XI2(I)/YZ.
C   YI=XI3(I)/YZ.
C   CALL ALIPEN (I,YI,XI1(I),XNM(I),XNP(I),XNM(I))

```

NTG 70  
 NTG 80  
 NTG 90  
 NTG 100  
 NTG 110  
 NTG 120

APA 10  
 APA 20  
 APA 30  
 APA 40  
 APA 50  
 APA 60  
 APA 70  
 APA 80  
 APA 90  
 APA 100  
 APA 110

PPRARA 120  
 VARA 130  
 ARA 140  
 ARA 150  
 ARA 160  
 ARA 170  
 ARA 180  
 ARA 190  
 ARA 200  
 ARA 210  
 ARA 220

ARA 230  
 ARA 240  
 ARA 250  
 ARA 260  
 ARA 270  
 ARA 280  
 ARA 290  
 ARA 300  
 ARA 310  
 ARA 320  
 ARA 330

ARA 340  
 ARA 350  
 ARA 360  
 ARA 370  
 ARA 380  
 ARA 390  
 ARA 400  
 ARA 410  
 ARA 420

ARA 430  
 ARA 440  
 ARA 450  
 ARA 460  
 ARA 470  
 ARA 480  
 ARA 490  
 ARA 500  
 ARA 510

ARA 520  
 ARA 530  
 ARA 540  
 ARA 550  
 ARA 560  
 ARA 570  
 ARA 580  
 ARA 590

```

CALL AITKEN (PHY,PRR,NPRF,1,IP,DP)
CALL AITKEN (PHY,PRR,NPRF,1,YM,DM)
DX=DP-DM
N=1
IF (I.GT.225) N=1
CALL AITKEN (DTY,XI1,NLN,N,YZ,P(1))
CALL AITKEN (DTY,XI2,NLN,N,YZ,P(2))
CALL AITKEN (DTY,XI3,NLN,N,YZ,P(3))
CALL AITKEN (DTY,XI4,NLN,N,YZ,P(4))
CALL CHECK (P,4,MFLAG)
J=4
P(5)=P(4)/5.
CALL AITKEN (DTY,VE1,NLN,N,YZ,V(1))
CALL AITKEN (DTY,VE2,NLN,N,YZ,V(2))
CALL AITKEN (DTY,VE3,NLN,N,YZ,V(3))
CALL AITKEN (DTY,VE4,NLN,N,YZ,V(4))
CALL CHECK (V,4,MFLAG)
V(5)=V(4)/5.
CALL AITKEN (DTR,P,J,N,XP,XNE)
CALL AITKEN (DTR,V,J,N,XP,VEE)
YZ=YZ+DY
AR=AR+SQRT(DX**2+DY**2)*6.2832*XP
AZ=AZ+SQRT(DX**2+DY**2)*6.2832*XP*XNE**2*VEE
102 AN=AN+SQRT(DX**2+DY**2)*6.2832*XP*XNE*VEE
C
C SECTION FOR GRIDS
C
P(1)=6.2832*DTR(1)*XI1(NLN)
P(2)=6.2832*DTR(2)*XI2(NLN)
P(3)=6.2832*DTR(3)*XI3(NLN)
P(4)=6.2832*DTR(4)*XI4(NLN)
CALL CHECK (P,4,MFLAG)
P(5)=0.
V(1)=VE1(NLN)
V(2)=VE2(NLN)
V(3)=VE3(NLN)
V(4)=VE4(NLN)
V(5)=0.
DO 103 JK=1,5
103 Q(JK)=V(JK)*P(JK)
CALL QTEG (DTR,Q,Z,5)
WRITE (6,108) Z(5)
I1=Z(5)
AN=AN+Z(5)
DO 104 JK=2,5
104 Q(JK)=Q(JK)*P(JK)/(6.2832*DTR(JK))
CALL QTEG (DTR,Q,Z,5)
I2=Z(5)
AZ=AZ+Z(5)
Z(5)=Z(5)*2.2828
WRITE (6,108) Z(5)
AR=AR+3.14159*DTR(5)**2
Q(5)=0.
C
C SECTION FOR RAFFLE
C
N=1
CALL AITKEN (DTY,XI1,NLN,N,DI,P(1))
CALL AITKEN (DTY,XI2,NLN,N,DI,P(2))
CALL AITKEN (DTY,XI3,NLN,N,DI,P(3))
CALL AITKEN (DTY,XI4,NLN,N,DI,P(4))
CALL CHECK (P,4,MFLAG)
CALL AITKEN (DTY,VE1,NLN,N,DI,V(1))
CALL AITKEN (DTY,VE2,NLN,N,DI,V(2))
CALL AITKEN (DTY,VE3,NLN,N,DI,V(3))
CALL AITKEN (DTY,VE4,NLN,N,DI,V(4))

```

```

ARA 600
ARA 610
ARA 620
ARA 630
ARA 640
ARA 650
ARA 660
ARA 670
ARA 680
ARA 690
ARA 700
ARA 710
ARA 720
ARA 730
ARA 740
ARA 750
ARA 760
ARA 770
ARA 780
ARA 790
ARA 800
ARA 810
ARA 820
ARA 830
ARA 840
ARA 850
ARA 860
ARA 870
ARA 880
ARA 890
ARA 900
ARA 910
ARA 920
ARA 930
ARA 940
ARA 950
ARA 960
ARA 970
ARA 980
ARA 990
ARA 1000
ARA 1010
ARA 1020
ARA 1030
ARA 1040
ARA 1050
ARA 1060
ARA 1070
ARA 1080
ARA 1090
ARA 1100
ARA 1110
ARA 1120
ARA 1130
ARA 1140
ARA 1150
ARA 1160
ARA 1170
ARA 1180
ARA 1190
ARA 1200
ARA 1210
ARA 1220
ARA 1230
ARA 1240
ARA 1250

```

```

CALL CHECK (V,4,MFLAG)
Q(1)=6.2832*QTR(1)*P(1)*V(1)
Q(2)=6.2832*QTR(2)*P(2)*V(2)
Q(3)=6.2832*QTR(3)*P(3)*V(3)
Q(4)=6.2832*QTR(4)*P(4)*V(4)
CALL QTRG (QTR,Q,2,5)
CALL AITKEN (QTR,2,5,1,R,EC)
DO 105 IJ=1,4
105 Q(IJ)=Q(IJ)*P(IJ)
CALL QTRG (QTR,Q,2,5)
CALL AITKEN (QTR,2,5,1,R,ED)
AR=AR+3.1416*R**2
AN=AN+EC
AZ=A7+ED
IF (IFLAG.NE.1) GO TO 106

C
C
C
CATHODE POLE PIECE SECTION

CALL AITKEN (QTY,XI1,NLN,N,CZU,P(1))
CALL AITKEN (QTY,XI2,NLN,N,CZU,P(2))
CALL AITKEN (QTY,XI3,NLN,N,CZU,P(3))
CALL AITKEN (QTY,XI4,NLN,N,CZU,P(4))
CALL CHECK (P,4,MFLAG)
P(5)=P(4)/5.
CALL AITKEN (QTR,P,5,N,R,XN1)
CALL AITKEN (QTY,VE1,NLN,N,CZU,V(1))
CALL AITKEN (QTY,VE2,NLN,N,CZU,V(2))
CALL AITKEN (QTY,VE3,NLN,N,CZU,V(3))
CALL AITKEN (QTY,VE4,NLN,N,CZU,V(4))
CALL CHECK (V,4,MFLAG)
V(5)=V(4)/5.
CALL AITKEN (QTR,V,5,N,R,VN1)
CALL AITKEN (QTY,XI1,NLN,N,CZD,P(1))
CALL AITKEN (QTY,XI2,NLN,N,CZD,P(2))
CALL AITKEN (QTY,XI3,NLN,N,CZD,P(3))
CALL AITKEN (QTY,XI4,NLN,N,CZD,P(4))
CALL CHECK (P,4,MFLAG)
P(5)=P(4)/5.
CALL AITKEN (QTR,P,5,N,R,XN2)
CALL AITKEN (QTY,VE1,NLN,N,CZD,V(1))
CALL AITKEN (QTY,VE2,NLN,N,CZD,V(2))
CALL AITKEN (QTY,VE3,NLN,N,CZD,V(3))
CALL AITKEN (QTY,VE4,NLN,N,CZD,V(4))
CALL CHECK (V,4,MFLAG)
V(5)=V(4)/5.
CALL AITKEN (QTR,V,5,N,R,VN2)
XL=CZU-CZD
AR=AR+XI*6.2832*R
XN=(XN1+XN2)/2.
VN=(VN1+VN2)/2.
AN=AN+6.2832*PI*XL*XN*VN
A7=A7+.62832*PI*XL*XN**2*VN

C
C
C
106 WRITE (6,113) AR
WRITE (6,112) AN
WRITE (6,114) A7
F1=AR*PI*FF/A7*VFA
F2=AN*PI*FF**2/A7*VFA
REF=2.924*PI/(I*XMFF)
WRITE (6,115) F1,F2,REF
WRITE (6,116) MFLAG
WRITE (6,117) MFLAG
WRITE (6,118)

```

```

ARA 1260
ARA 1270
ARA 1280
ARA 1290
ARA 1300
ARA 1310
ARA 1320
ARA 1330
ARA 1340
ARA 1350
ARA 1360
ARA 1370
ARA 1380
ARA 1390
ARA 1400
ARA 1410
ARA 1420
ARA 1430
ARA 1440
ARA 1450
ARA 1460
ARA 1470
ARA 1480
ARA 1490
ARA 1500
ARA 1510
ARA 1520
ARA 1530
ARA 1540
ARA 1550
ARA 1560
ARA 1570
ARA 1580
ARA 1590
ARA 1600
ARA 1610
ARA 1620
ARA 1630
ARA 1640
ARA 1650
ARA 1660
ARA 1670
ARA 1680
ARA 1690
ARA 1700
ARA 1710
ARA 1720
ARA 1730
ARA 1740
ARA 1750
ARA 1760
ARA 1770
ARA 1780
ARA 1790
ARA 1800
ARA 1810
ARA 1820
ARA 1830
ARA 1840
ARA 1850
ARA 1860
ARA 1870
ARA 1880
ARA 1890
ARA 1900
ARA 1910

```

```

107 FORMAT (2I5,4F10.4)
108 FORMAT (2X, 5HI (CM-1)=,F11.4)
109 FORMAT (2X, 40HNEGATIVE VELOCITY EXTRAPOLATION OCCURRED,15, 7H TARI
      1TIMES)
110 FORMAT (10X,8(F10.3,2X))
111 FORMAT (HF10.6)
112 FORMAT (3X, 13HAN (CM2/CM3)=,F11.4)
113 FORMAT (3X, 9HAR (CM2)=,F11.4)
114 FORMAT (3X, 13HAZ (CM2/CM5)=,F11.4)
115 FORMAT (2X, 3HF1=,F10.4,2X, 3HF2=,F10.4,2X, 13HI+*/I+ FACTOR,F10.4
      1.4)
116 FORMAT (2X, 39HNEGATIVE DENSITY EXTRAPOLATION OCCURRED,15, 8H TARI
      1TIMES)
C
      END
      SUBROUTINE CHECK (P,N,NFLAG)
      DIMENSION P(N)
      DO 101 J=1,N
        IF (P(J).GE.0.0) GO TO 101
        P(J)=0.0
        NFLAG=NFLAG+1
101 CONTINUE
      RETL,P,N
C
      END
      #

```

```

ARA 1920
ARA 1930
ARA 1940
ARA 1950
ARA 1960
ARA 1970
ARA 1980
ARA 1990
ARA 2000
ARA 2010
ARA 2020
ARA 2030
ARA 2040
ARA 2050
ARA 2060
CK 10
CK 20
CK 30
CK 40
CK 50
CK 60
CK 70
CK 80
CK 90
CK 100

```